

Article

# Poly (Vinyl Alcohol) Hydrogels Boosted with Cross-Linked Chitosan and Silver Nanoparticles for Efficient Adsorption of Congo Red and Crystal Violet Dyes

Reem T. Alfuraydi <sup>1,\*</sup>, Nouf F. Al-Harby <sup>1</sup> , Fahad M. Alminderej <sup>1</sup> , Noura Y. Elmehbad <sup>2</sup>   
and Nadia A. Mohamed <sup>1,3,\*</sup> 

<sup>1</sup> Department of Chemistry, College of Science, Qassim University, Buraidah 51452, Saudi Arabia; hrbien@qu.edu.sa (N.F.A.-H.); f.alminderej@qu.edu.sa (F.M.A.)

<sup>2</sup> Department of Chemistry, Faculty of Science and Arts, Najran University, Najran 55461, Saudi Arabia; nyalmehbad@nu.edu.sa

<sup>3</sup> Department of Chemistry, Faculty of Science, Cairo University, Giza 12613, Egypt

\* Correspondence: r.alfuraydi@qu.edu.sa (R.T.A.); na.ahmed@qu.edu.sa or nahmed@sci.cu.edu.eg (N.A.M.)

**Abstract:** In our previous work, three different weight ratios of chitosan/PVA (1:3, 1:1, and 3:1) were blended and then cross-linked with trimellitic anhydride isothiocyanate (TAI) at a concentration depending on their chitosan content, obtaining three hydrogels symbolized by H<sub>13</sub>, H<sub>11</sub>, and H<sub>31</sub>. Pure chitosan was cross-linked with TAI, producing a hydrogel symbolized by H<sub>10</sub>. Further, three H<sub>31</sub>-based silver nanoparticles composites (H<sub>31</sub>/AgNPs1%, H<sub>31</sub>/AgNPs3%, and H<sub>31</sub>/AgNPs5%) were also synthesized. They were investigated, for the first time in this study, as adsorbents for Congo Red (CR) and Crystal Violet (CV) dyes. The removal efficiency of CR dye increased with increasing H<sub>10</sub> content in the hydrogels, and with increasing AgNP content in the composites, reaching 99.91% for H<sub>31</sub>/AgNPs5%. For CV dye, the removal efficiency increased with the increase in the PVA content. Furthermore, the removal efficiency of CV dye increased with an increasing AgNP content, reaching 94.7% for H<sub>31</sub>/AgNPs5%. The adsorption capacity increased with the increase in both the initial dye concentration and temperature, while with an increasing pH it increased in the case of CV dye and decreased in the case of CR dye. The adsorption of CV dye demonstrated that the Freundlich isotherm model is better suited for the experimental results. Moreover, the results were best fitted with pseudo-second-order kinetic model.

**Keywords:** PVA/chitosan blend-based hydrogels; cross-linking; silver nano bio-composites; adsorption studies; Congo Red dye; Crystal Violet dye



**Citation:** Alfuraydi, R.T.; Al-Harby, N.F.; Alminderej, F.M.; Elmehbad, N.Y.; Mohamed, N.A. Poly (Vinyl Alcohol) Hydrogels Boosted with Cross-Linked Chitosan and Silver Nanoparticles for Efficient Adsorption of Congo Red and Crystal Violet Dyes. *Gels* **2023**, *9*, 882. <https://doi.org/10.3390/gels9110882>

Academic Editor: Bowen Yao

Received: 7 October 2023

Revised: 25 October 2023

Accepted: 2 November 2023

Published: 7 November 2023



**Copyright:** © 2023 by the authors. Licensee MDPI, Basel, Switzerland. This article is an open access article distributed under the terms and conditions of the Creative Commons Attribution (CC BY) license (<https://creativecommons.org/licenses/by/4.0/>).

## 1. Introduction

The drainage of the synthetic dye-containing effluents into the resources of water causes great anxiety because these dyes are very stable, highly toxic, and have the propensity for accumulation in the environment, threatening the life of both human beings and aquatic organisms. Contact with these dyes leads to conjunctivitis, asthma, rhinitis, and dermatitis, in addition to other allergy diseases [1]. Thus, these dyes should be removed before drainage into water resources, and this is considered one of the main universal environmental requirements [2].

Various methods have been applied for treating these effluents using ion exchangers, membranes for filtration, and bio-degradative, coagulating, flocculating, chemical precipitating, photo-degradative, oxidizing, and ozonizing agents [2,3]. Regardless of the good efficiency of these methods on the industrial level, there are some issues facing their application, such as the high consumption of energy, the high price of utilized chemicals, undesirable toxic by-products, and the poor performance of the dyes at a low concentration [3,4]. Nowadays, the adsorption method is a highly effective technique for

dye removal due to its high efficiency, simplicity, rapidness, easy operation, low initial cost, adsorbent abundance, lack of undesirable secondary products, and the easy restoration of the adsorbents for reuse [5].

Poly (vinyl alcohol), PVA, an eco-friendly synthetic vinyl polymer, showed some unique physicochemical and mechanical features such as flexibility, water solubility, hydrophilicity, chemical stability, high tensile strength, inherent non-toxicity, non-carcinogenicity, biocompatibility, bio-degradability, elasticity, and film and gel forming ability [6]. It has numerous biomedical, industrial and environmental applications since it is used as a basic material for replacing skin and the cartilage, vocal cord reconstruction, and contact lenses and as a better adsorbent of cationic dyes than anionic ones [7,8]. Thus, the enhancement of its adsorption capability toward anionic dyes is considered to be a desired approach for extending its application fields. Hence, its incorporation with another polymer with a high adsorption capacity for anionic dyes, such as chitosan, is deemed a key to the enhancement of its adsorption capability for anionic dyes.

Chitosan, an eco-friendly natural biopolymer, has various intriguing properties; it is renewable, abundant, non-toxic, highly viscous, a film forming-material, an antioxidant agent, an antimicrobial agent, a hypolipidemic agent, highly polyelectrolytic, a binder for metals, fats, and anionic dyes, bio-degradable, bio-compatible, and a wound healing accelerator. Thus, it could be utilized in the medicinal, industrial, and wastewater remediation fields [9–11]. Chitosan comes with a main issue, which is its high solubility in aqueous acids due to the formation of its protonated state. This restricts its use as an adsorbent for dyes since their effluents are usually acidic. Thus, it should be chemically modified to improve its stability in acidic media and make it a superb option as an adsorbent for dyes. Modification was achieved via the insertion of functional groups into its structure [12,13]; via grafting using functionalizing monomers [14]; through the polymer blending [15]; and via the incorporation of chemical cross-linkers [16–18].

Chitosan nanofiber membranes were fabricated by blending chitosan with PVA [15]. They were used as green adsorbents to withdraw CR dye from an aqueous solution. The adsorption capacity increased with an increase in the degree of deacetylation of chitosan. The Langmuir isotherm model and the pseudo-second-order kinetic model could accurately represent the adsorption process. This shows that chemical adsorption could be a rate-limiting phase and that  $358 \text{ mg L}^{-1}$  was the greatest adsorption capacity.

PVA/chitosan nanofiber mats improved with aluminum–cerium spinel oxide ( $\text{CeAlO}_3$ ) nanoparticles showed a better uptake for Methylene Blue (MB) dye, and was fitted to the pseudo-second-order kinetic model. The maximum adsorption capacity of MB dye was 817.81 and 714.61 mg/g for modified and virgin nanofibers, respectively [19]. The maximum adsorption capacity of a PVA/chitosan-based adsorbent film to remove Acid Orange 7 was 678 mg/g at 298 K and pH = 2.5. The adsorption was suitable to the Lagergren pseudo first-order kinetic model and was described using the Redlich–Peterson model [20].

A PVA/chitosan mixture nanofiber was used to adsorb Direct Red 80, Direct Red 81, and Reactive Red 180 dyes. The adsorption increased as the pH decreased and conformed to the pseudo-second-order kinetic model. This occurred at the specific homogeneous sites of the nanofiber blend (Langmuir model) [21].

Previously, we modified chitosan via a reaction of its  $-\text{NH}_2$  groups with TAI, achieving the inclusion of both the amide, thiourea, carboxylic groups in addition to the residual  $-\text{NH}_2$  groups in it. This remarkably boosted the removal of both the anionic CR and the cationic Basic Red 12 (BR 12) dyes by the obtained chitosan hydrogels [22–24]. Based on these findings, we have progressed in the preparation of another series of PVA/chitosan blend-based hydrogels. Both TAI and silver nanoparticles (AgNPs) were employed to develop their features as antimicrobial agents and as inhibitors for biofilm formation [25]. Thus, we anticipate that this series of PVA/chitosan blend-based hydrogels and AgNP bio-composites will possess a better adsorption capacity for both anionic and cationic dyes, according to their contents of PVA, cross-linked chitosan, and AgNPs. Therefore, in this research, our objective was to study the isotherm properties, kinetics, and optimization of

the adsorption process of these hydrogels and AgNP bio-composites for the removal of CR and CV dyes. The effect of temperature, initial dye concentration, pH, PVA/cross-linked chitosan ratio (cross-linking moiety proportions), and AgNP content on the adsorption process was also evaluated. Further, the possibility of regenerating the prepared adsorbents for their reuse was investigated.

## 2. Results and Discussion

### 2.1. Removal of the CR and CV Dyes

The expansion of the numerous industrial activities that mainly use dyes, such as those of the fabric, cosmetic, leather, food, printing, plastic, and paper industries, has resulted in the discharge of large amounts of colored effluents into the aquatic environment. This is a great public problem and one of the major threats not only to human beings but also to all aquatic creatures due to the hazardous nature of synthetic dyes, which is correlated with their high toxicity and high resistance against environmental factors such as heat, light, and microorganisms resulting from their complicated aromatic structures. Even low concentrations of these dyes lead to an unacceptable coloration of water, causing aesthetic problems, the prevention of light and oxygen from reaching aquatic living organisms, and the lowering of their photosynthetic activities, in addition to causing severe damage to the liver and the digestive and central nervous system in humans [26]. With respect to this concern, the removal of CR and CV dyes, as representative examples of anionic and the cationic dyes, respectively, from their aqueous solutions before they are discharged into the environment is one of the prime global environmental interests. Adsorbents based on chitosan showed a higher adsorption capacity for various dyes [27].

The results of the adsorption capacity ( $q_e$ , Equation (1)) for different CR dye concentrations, at 25 and 50 °C, and at pH 7, for the prepared hydrogels and the H<sub>31</sub>/AgNP composites are shown in Figures 1 and 2, respectively.

In accordance with the adsorption capacity, the effectiveness of the investigated hydrogels and the H<sub>31</sub>/AgNP composites for CR dye (Figures 1 and 2) can be arranged as follows: PVA < H<sub>13</sub> < chitosan < H<sub>11</sub> < H<sub>10</sub> < H<sub>31</sub> < H<sub>31</sub>/AgNPs1% < H<sub>31</sub>/AgNPs3% < H<sub>31</sub>/AgNPs5%. For example, at a 18 mg L<sup>-1</sup> dye concentration and at 25 °C and pH 7, the adsorption capacities for the CR dye of PVA, H<sub>13</sub>, chitosan, H<sub>11</sub>, H<sub>10</sub>, H<sub>31</sub>, H<sub>31</sub>/AgNPs1%, H<sub>31</sub>/AgNPs3%, and H<sub>31</sub>/AgNPs5% were 6.20, 10.80, 11.20, 12.00, 12.50, 13.20, 15.80, 16.90, and 17.74 mg g<sup>-1</sup>, respectively.

The % efficiency (Equation (3)) of the removal of CR dye by these hydrogels and the H<sub>31</sub>/AgNP composites at a 18 mg L<sup>-1</sup> dye concentration, at 25 and 50 °C, and at pH 7 is summarized in Table 1. Notably, the % removal efficiency for CR dye can also be arranged as follows: PVA < H<sub>13</sub> < chitosan < H<sub>11</sub> < H<sub>10</sub> < H<sub>31</sub> < H<sub>31</sub>/AgNPs1% < H<sub>31</sub>/AgNPs3% < H<sub>31</sub>/AgNPs5%. For example, at a 18 mg L<sup>-1</sup> dye concentration at 25 °C, and at pH 7 (Table 1), the % efficiency of the removal of CR dye by PVA, H<sub>13</sub>, chitosan, H<sub>11</sub>, H<sub>10</sub>, H<sub>31</sub>, H<sub>31</sub>/AgNPs1%, H<sub>31</sub>/AgNPs3%, and H<sub>31</sub>/AgNPs5% was 34.69, 60.00, 62.22, 66.70, 69.40, 73.33, 87.78, 93.89, and 98.54%, respectively.

**Table 1.** The efficiency (%) of the prepared hydrogels and the H<sub>31</sub>/AgNP composites for CR dye, at 25 and 50 °C, at an initial dye concentration of 18 mg L<sup>-1</sup>, and at pH 7.

Temperature	PVA	Chitosan	H <sub>10</sub>	H <sub>11</sub>	H <sub>13</sub>	H <sub>31</sub>	H <sub>31</sub> /AgNPs1%	H <sub>31</sub> /AgNPs3%	H <sub>31</sub> /AgNPs5%
25 °C	34.69	62.22	69.40	66.70	60.00	73.33	87.78	93.89	98.54
50 °C	37.50	84.03	96.80	90.30	76.57	99.61	99.61	99.62	99.91

PVA showed a lower adsorption capacity and a weaker removal efficiency for anionic CR dye than did chitosan due to the acidic and the basic nature of PVA and chitosan, respectively. On the other hand, H<sub>10</sub> displayed a better adsorption capacity and a higher removal efficiency for CR dye than did chitosan due to the incorporation of additional basic groups (thiourea and amide linkages) into chitosan after its cross-linking process. Thus,

the adsorption capacity and the removal efficiency of the prepared hydrogels for CR dye increased with an increasing  $H_{10}$  content, i.e., from  $H_{13}$  to  $H_{31}$ . This is due to the increased number of incorporated thiourea and amide moieties into chitosan after the cross-linking process, from  $H_{13}$  to  $H_{31}$ , which work as efficient binding sites for the CR anionic dye. Thus, the incorporation of  $H_{10}$  with PVA improves the adsorption capacity and the removal efficiency for CR dye, reaching their maximum in  $H_{31}$  [28]. Further, the dispersion of AgNPs into the matrices of  $H_{31}$  improved the adsorption capacity of the produced composites relative to that of  $H_{31}$  due to the increased surface area and the additional cross-linking between the electron-rich nitrogen and oxygen atoms of the hydrogel components and AgNPs [29,30].

The results of the capacity ( $q_e$ , Equation (1)) for adsorption of the CV dye onto the prepared hydrogels and the  $H_{31}$ /AgNP composites at different dye concentrations, at 25 and 50 °C, and at pH 7 are shown in Figures 3 and 4, respectively.

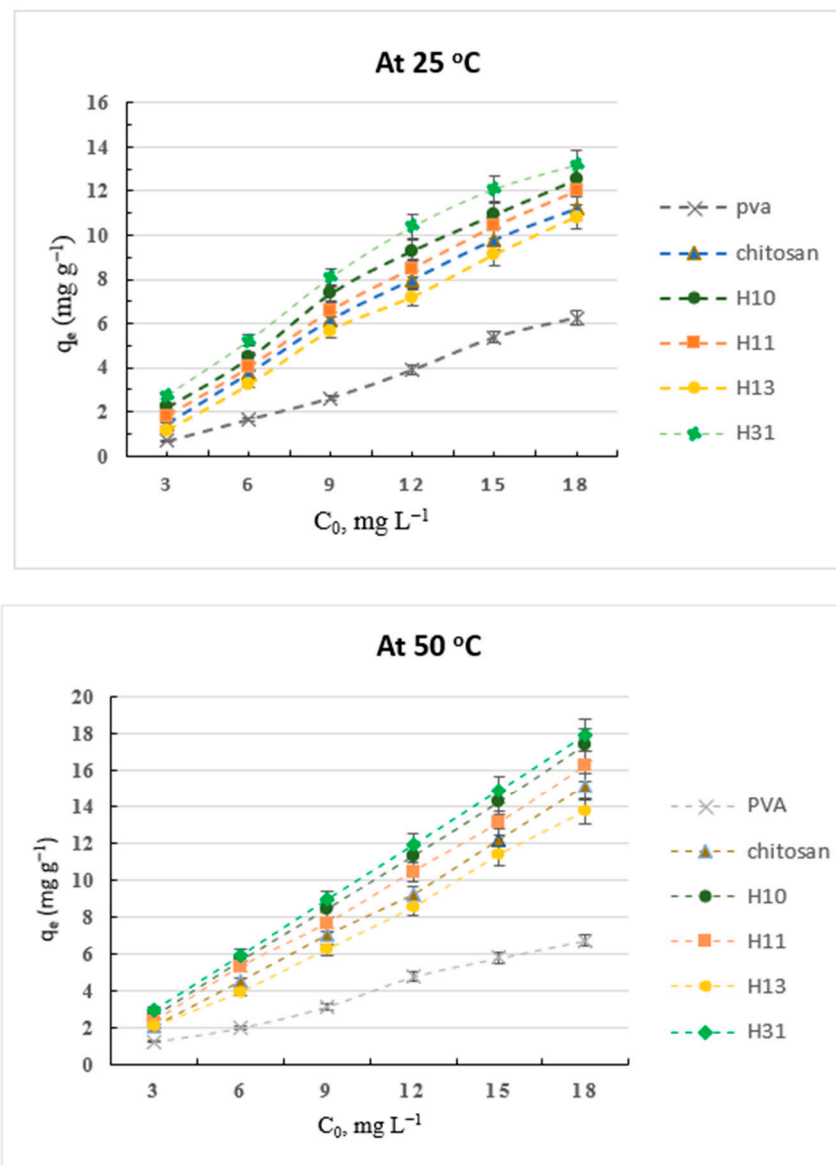


**Figure 1.** The capacity of CR dye to adsorb onto the prepared hydrogels at different dye concentrations, and at pH 7.

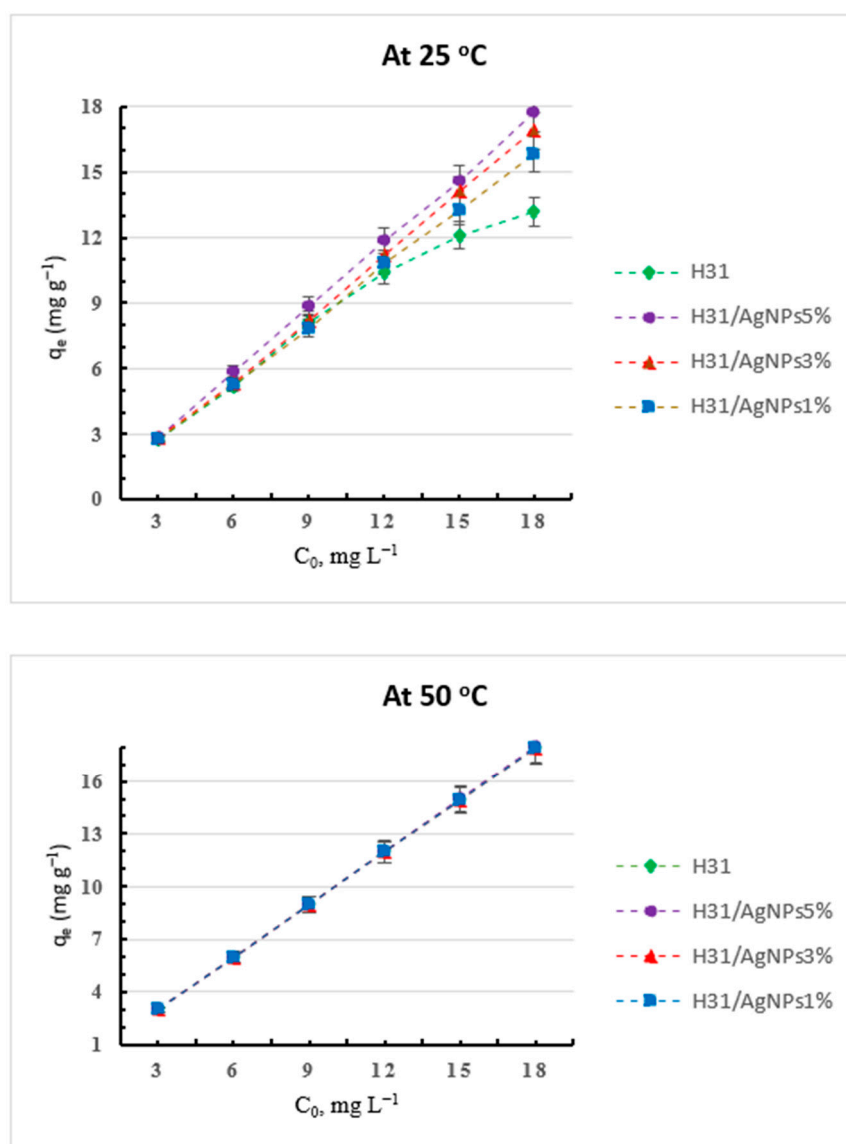


**Figure 2.** The capacity of CR dye to adsorb onto H<sub>31</sub> and H<sub>31</sub>/AgNP composites at different dye concentrations, and at pH 7.

Chitosan showed a lower adsorption capacity and a weaker removal efficiency for the basic CV dye than did PVA due to the basic and the acidic nature of chitosan and PVA, respectively, since PVA possesses a lot of hydroxyl groups which act as adsorption sites for the cationic dyes, while H<sub>10</sub> displayed a better adsorption capacity and a higher removal efficiency for the CV dye than did chitosan due to the incorporation of the additional acidic carboxylic groups into chitosan, after its cross-linking process, which work as efficient binding sites for the CV cationic dye. Thus, the adsorption capacity and removal efficiency for the CV dye of the prepared hydrogels increased with the increase in their PVA content, i.e., from H<sub>31</sub> to H<sub>13</sub>. Thus, the incorporation of PVA with H<sub>10</sub> improved the adsorption capacity and the removal efficiency for CV dye, reaching the maximum in H<sub>13</sub> [31]. Further, the loading of AgNPs inside the H<sub>31</sub> matrices enhanced the adsorption efficiencies of the resulting composites in comparison to that of H<sub>31</sub> due to the increased surface area, in addition to the many cross-linkages that originate between the AgNPs and the electron-rich nitrogen and oxygen atoms of the components of the hydrogels [29,30].

The adsorption capacity for both the CR and the CV dyes of the prepared hydrogels and the H<sub>31</sub>/AgNP composites are greatly dependent on the initial concentration of the dye. Their adsorption capacity increased with an increasing initial dye concentration from 3

to  $18 \text{ mg L}^{-1}$  and from 2 to  $12 \text{ mg L}^{-1}$  of the CR and the CV dyes, respectively (Figures 1–4). For example, at  $50 \text{ }^\circ\text{C}$ , the adsorption capacity of  $\text{H}_{31}/\text{AgNPs}5\%$  was 3.00, 5.96, 8.99, 11.96, 14.94, and  $17.93 \text{ mg g}^{-1}$  with the use of CR dye at initial concentrations of 3, 6, 9, 12, 15, and  $18 \text{ mg L}^{-1}$ , respectively (Figure 2). Furthermore, at  $50 \text{ }^\circ\text{C}$ , the adsorption capacity of  $\text{H}_{31}/\text{AgNPs}5\%$  was 1.97, 3.83, 5.88, 7.41, 9.51, and  $11.37 \text{ mg g}^{-1}$  when using CV dye at initial concentrations of 2, 4, 6, 8, 10, and  $12 \text{ mg L}^{-1}$ , respectively (Figure 4). The impact of the initial concentration of the dye is based on the direct relationship between the dye's concentration and the convenient sites on the surfaces of the adsorbents. An increase in the initial concentration of the dyes leads to an increase in the capacity of the adsorbents due to the great driving forces for the transfer of mass at a high initial concentration of the dye [32].

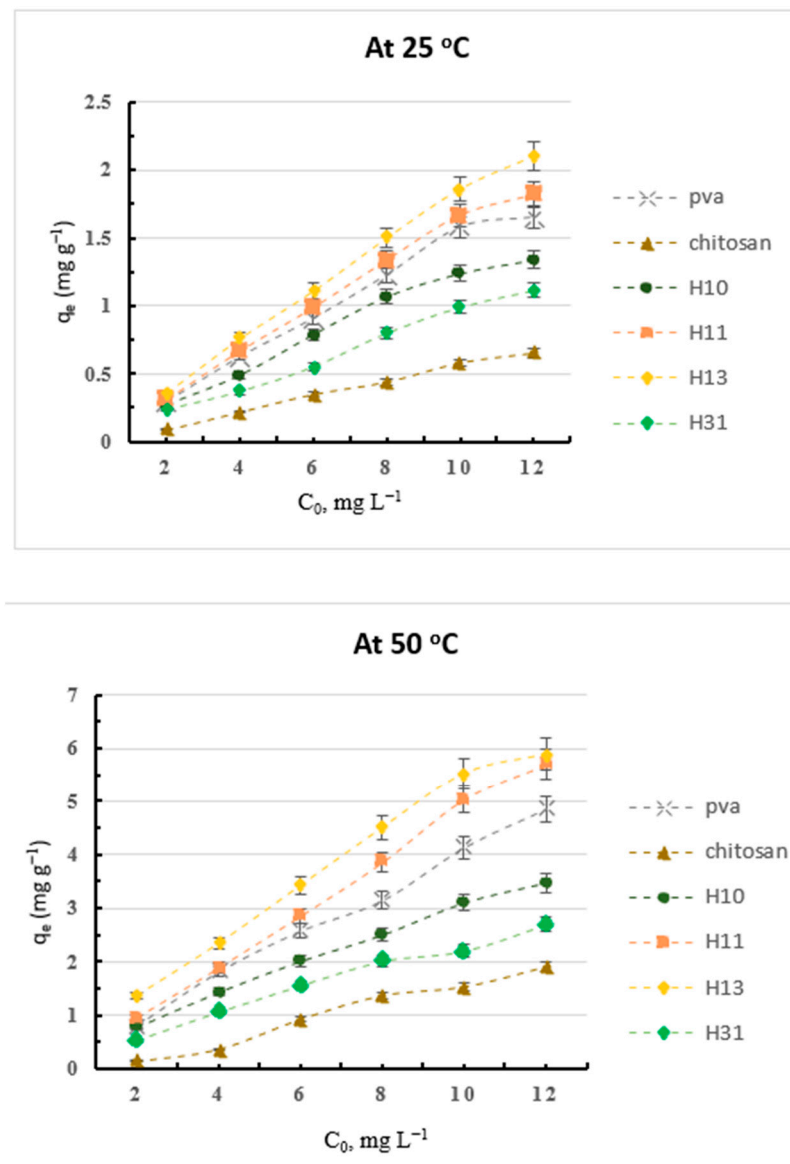


**Figure 3.** The adsorption capacity of CV dye onto the prepared hydrogels at different dye concentrations, and at pH 7.

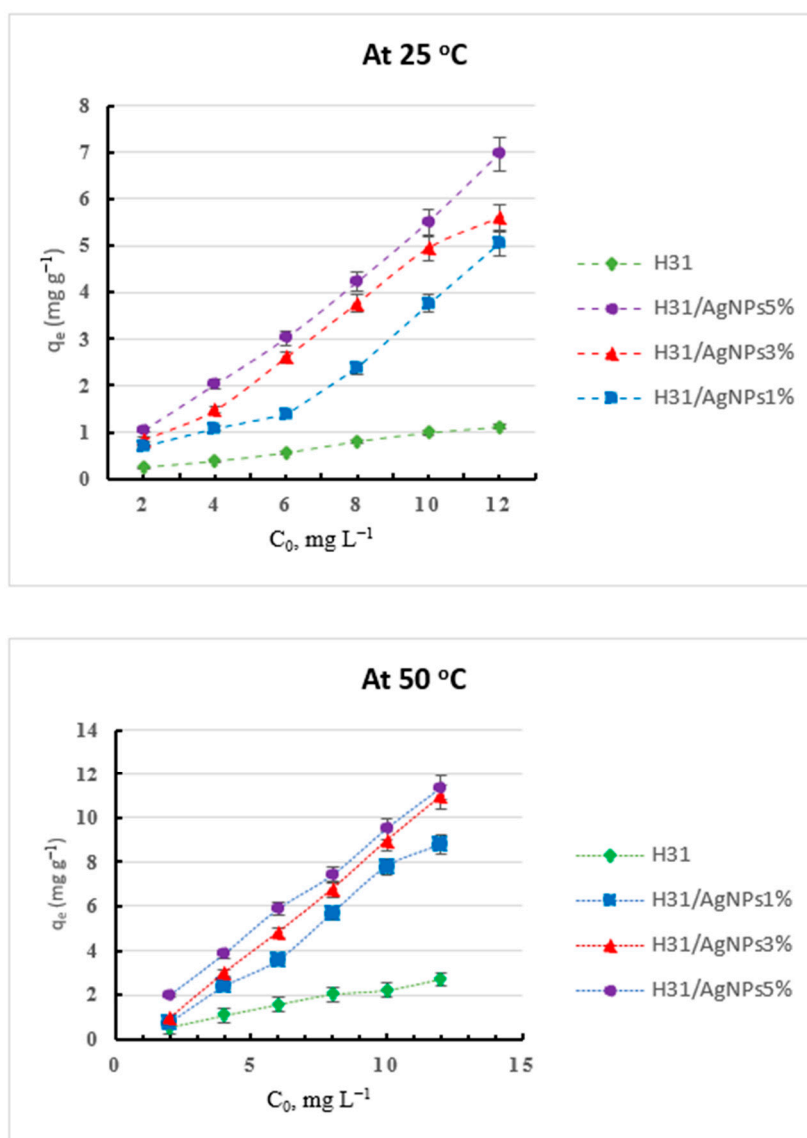


**Figure 4.** The adsorption capacity of the CV dye onto the H<sub>31</sub> and H<sub>31</sub>/AgNP composites at different dye concentrations, and at pH 7.

Contrary to the results of the CR anionic dye, in accordance with the adsorption capacity, at all the used temperatures and different dye concentrations, the effectiveness of the prepared hydrogels and the H<sub>31</sub>/AgNP composites toward the adsorption of the CV cationic dye (Figures 3 and 4) can be classified as follows: chitosan < H<sub>31</sub> < H<sub>10</sub> < PVA < H<sub>11</sub> < H<sub>13</sub> < H<sub>31</sub>/AgNPs1% < H<sub>31</sub>/AgNPs3% < H<sub>31</sub>/AgNPs5%. For example, at a 12 mg L<sup>-1</sup> dye concentration, at 50 °C, and at pH 7, the adsorption capacities for CV dye of chitosan, H<sub>31</sub>, H<sub>10</sub>, PVA, H<sub>11</sub>, H<sub>13</sub>, H<sub>31</sub>/AgNPs1%, H<sub>31</sub>/AgNPs3%, and H<sub>31</sub>/AgNPs5% were 1.91, 2.70, 3.47, 4.86, 5.70, 5.89, 8.78, 10.94, and 11.37 mg g<sup>-1</sup>, respectively. The % removal efficiency (Equation (3)) for CV dye of these hydrogels and the H<sub>31</sub>/AgNP composites at a 12 mg L<sup>-1</sup> dye concentration, at 25 and 50 °C, and at pH 7 is summarized in Table 2. Notably, the % removal efficiency for CV dye of these hydrogels and the H<sub>31</sub>/AgNP composites can also be arranged as follows: chitosan < H<sub>31</sub> < H<sub>10</sub> < PVA < H<sub>11</sub> < H<sub>13</sub> < H<sub>31</sub>/AgNPs1% < H<sub>31</sub>/AgNPs3% < H<sub>31</sub>/AgNPs5%. For example, at a 12 mg L<sup>-1</sup> dye concentration, at 50 °C, and at pH 7, the % removal efficiency for the CV dye of chitosan, H<sub>31</sub>, H<sub>10</sub>, PVA, H<sub>11</sub>, H<sub>13</sub>, H<sub>31</sub>/AgNPs1%, H<sub>31</sub>/AgNPs3%, and H<sub>31</sub>/AgNPs5% was 15.88, 22.50, 28.90, 40.46, 47.50, 49.08, 73.17, 91.18, and 94.71%, respectively.

**Table 2.** The removal efficiency (%) for CV dye of the prepared hydrogels and the H<sub>31</sub>/AgNP composites at 25 and 50 °C, at an initial dye concentration of 12 mg L<sup>-1</sup>, and at pH 7.

Temperature	PVA	Chitosan	H <sub>10</sub>	H <sub>11</sub>	H <sub>13</sub>	H <sub>31</sub>	H <sub>31</sub> /AgNPs1%	H <sub>31</sub> /AgNPs3%	H <sub>31</sub> /AgNPs5%
25 °C	13.75	5.42	11.17	15.17	17.50	9.28	42.05	46.62	58.04
50 °C	40.46	15.88	28.90	47.50	49.08	22.50	73.17	91.18	94.71

Further, the capacity for the adsorption of CR and CV dyes onto the prepared hydrogels and the H<sub>31</sub>/AgNP composites increased with an increase in temperature from 25 to 50 °C (Figures 1 and 4). This is ascribed to that an increase in the adsorption temperature, which enhanced the swelling ability inside the adsorbents, expediting dye molecule penetration inside the adsorbents. Further, the mobility of the dye molecules increased as the temperature of the adsorption process increased. This is well in agreement with the adsorption of CR dye by chitosan modified with terephthaloyl diisothiocyanate as a cross-linker [5].

The impact of variance in the pH of the CR dye solution (4, 7, and 9) at 25 °C on the adsorption behavior (Equation (1)) of H<sub>13</sub>, as a representative example of the investigated hydrogels, is shown in Figure 5. The importance of the role that pH plays in the adsorption process was clearly revealed, because the adsorption capacity,  $q_e$ , at pH 4 (the acidic medium) was higher than that at pH 7 and 9 (neutral and the basic media). This is ascribed to the fact that, in the acidic medium, the protonated groups of H<sub>13</sub> (NH<sub>3</sub><sup>+</sup>, NH<sub>2</sub><sup>+</sup>, OH<sub>2</sub><sup>+</sup>, C=OH<sup>+</sup>, and C=SH<sup>+</sup>) electrostatically interacted with the anionic groups of CR dye [33], in addition to  $\pi$ - $\pi$  stacking resulting from the interaction between the  $\pi$  bonds of the aromatic rings of CR dye and the  $\pi$  bonds of the aromatic rings of cross-linking moieties, and the hydrogen bond formation between the amino groups of the CR dye and the hydroxyl groups of PVA, leading to a synergistic effect by which CR dye was adsorbed onto the prepared hydrogels as shown in Scheme 1. It is worth mentioning that the pH<sub>zpc</sub> value refers to the fact that the surface of the adsorbent had positive charges at low pH values (online Supplemental File S1).

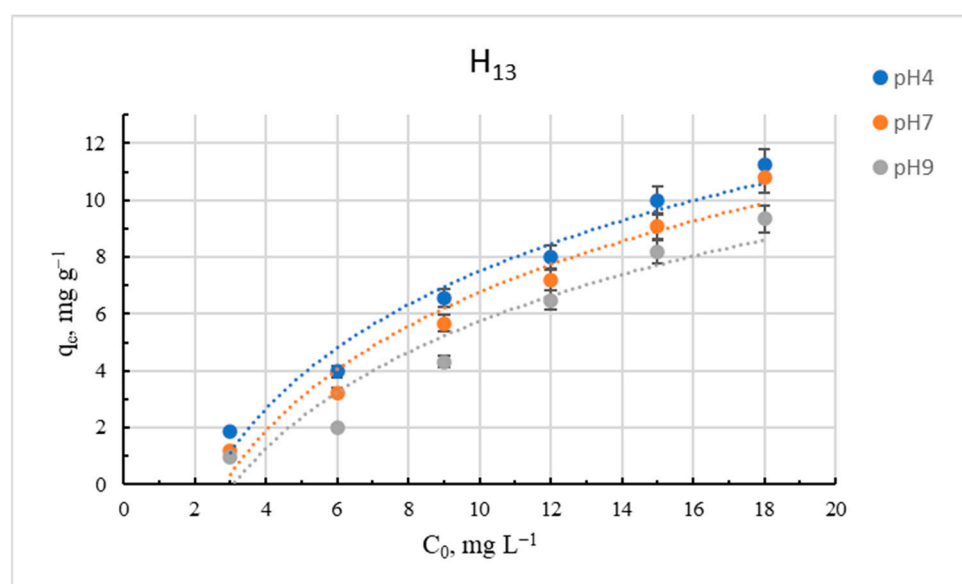
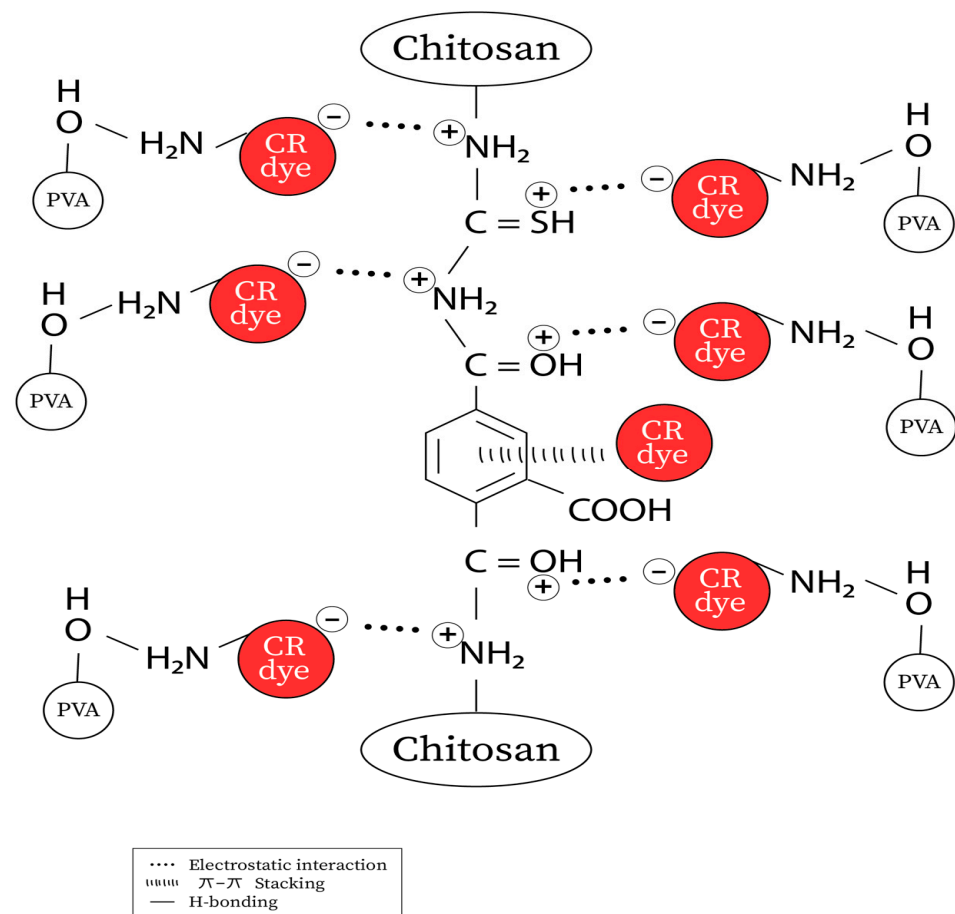


**Figure 5.** The capacity of CR dye to adsorb onto H<sub>13</sub> at different dye concentrations, at different pHs, and at 25 °C.



**Scheme 1.** The proposed adsorption mechanism for CR dye of the prepared hydrogels at pH 4.

The effect of differences in the pH of the CV dye solution (4, 7, and 9) at 25 °C on the adsorption behavior (Equation (1)) of H<sub>31</sub>, as a representative example of the investigated hydrogels, is shown in Figure 6. It can be noted that the adsorption capacity,  $q_e$ , at pH 9 (the basic medium) was higher than that at pH 7 and 4 (the neutral and the acidic media). This can be attributed to the fact that, in the basic medium, the deprotonated  $-\text{COOH}$  and  $-\text{OH}$  groups electrostatically interacted with the cationic groups of CV dye [34,35], in addition to  $\pi$ - $\pi$  stacking resulting from the interaction between the  $\pi$  bonds of the aromatic rings of CV dye and the  $\pi$  bonds of the aromatic rings of the cross-linking moieties, leading to a synergistic effect by which CV dye was adsorbed onto the prepared hydrogels, as shown in Scheme 2. It is worth mentioning that the pH<sub>Zpc</sub> value suggests that the surface of the adsorbent have negative charges at high pH values) online Supplemental File-S2).

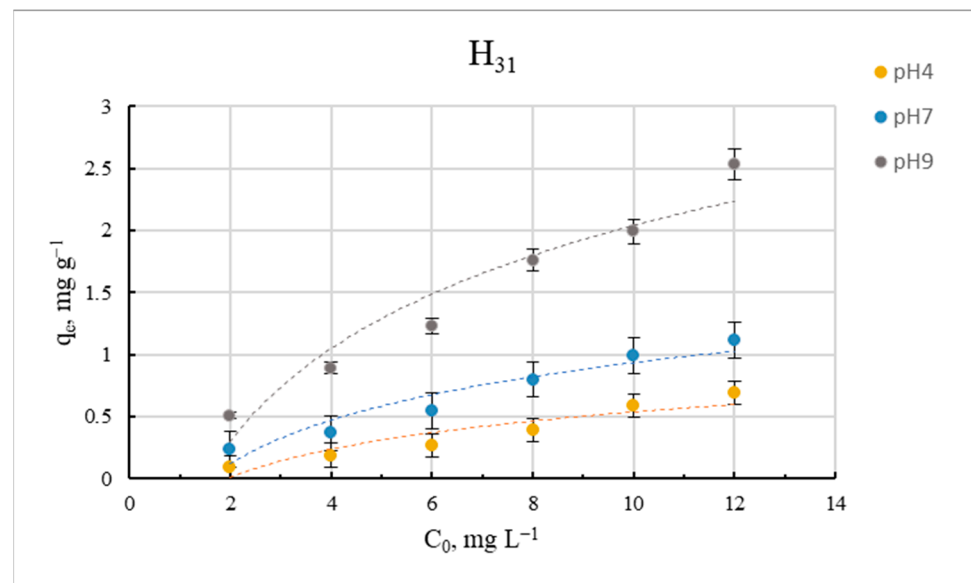
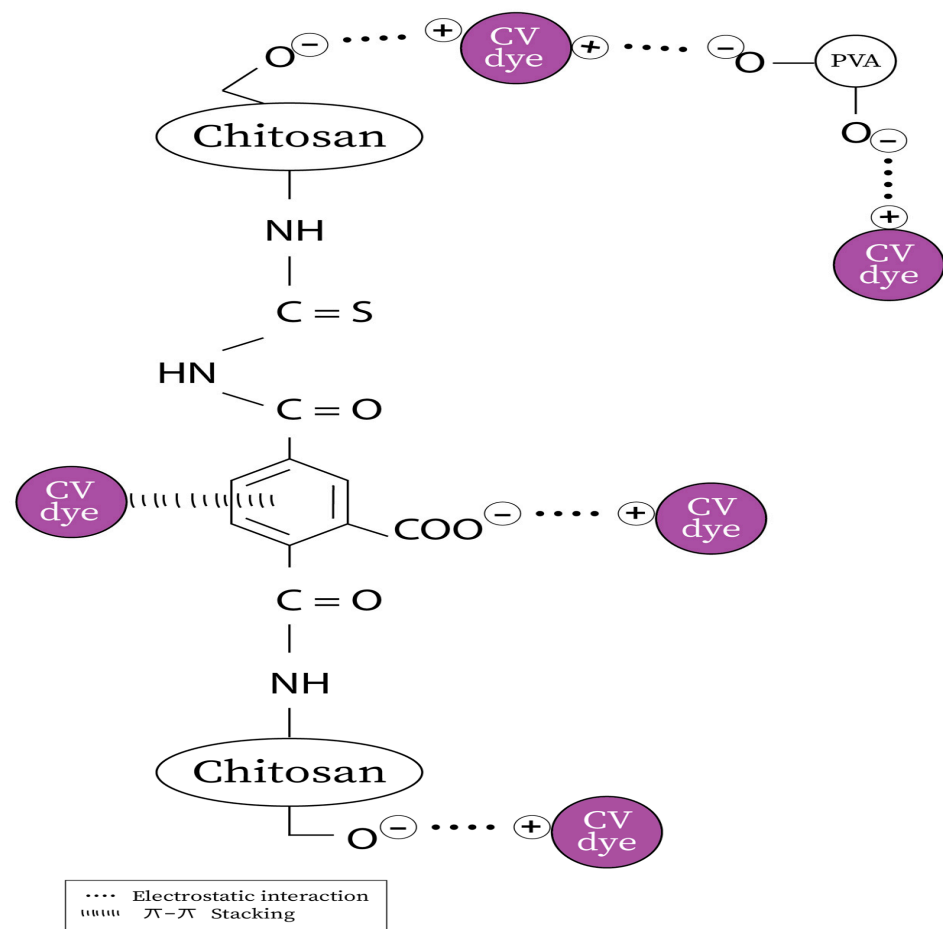


**Figure 6.** The capacity of CV dye to adsorb onto H<sub>31</sub> at different dye concentrations, at different pHs, and at 25 °C.



**Scheme 2.** The proposed adsorption mechanism for CV dye of the prepared hydrogels at pH 9.

## 2.2. Adsorption Isotherm Models

Online Supplemental Files S3 and S4, and Figures 7 and 8 show the Langmuir and the Freundlich adsorption isotherms of CV dye adsorbed onto the prepared hydrogels

and the H<sub>31</sub>/AgNP composites, and the adsorption isotherm parameters are listed in Tables 3 and 4. The regression coefficient ( $R^2$ ) values of the hydrogels and the H<sub>31</sub>/AgNP composites obtained from the Freundlich model at 50 °C ranged from 0.893 to 0.999 and from 0.857 to 0.863, respectively, which were much higher than those obtained from the Langmuir model, which ranged from 0.010 to 0.891 for the hydrogels and from 0.067 to 0.757 for the H<sub>31</sub>/AgNP composites. This indicates that the Freundlich model fitted better to the experimental results since the Freundlich isotherm assumes that multilayer adsorption and the adsorption occurs on heterogeneous surfaces [36]. The  $1/n$  values for the hydrogels (0.69–0.99) indicated that this isotherm was favorable while the values of  $1/n$  for the H<sub>31</sub>/AgNP composites were greater than unity, evidencing a favorable adsorption of the CV dye by the H<sub>31</sub>/AgNP composites, which could have occurred due to cooperative adsorption among the active sites with the different adsorption capacities (energies). Thus, there are considerable interactions among the solute molecules, increasing the adsorption efficiency with the increase in the solute concentration in the solution. This reinforces the belief that adsorption possibly occurs on multiple layers, which is obvious proof of mostly a physical adsorption mechanism [37].

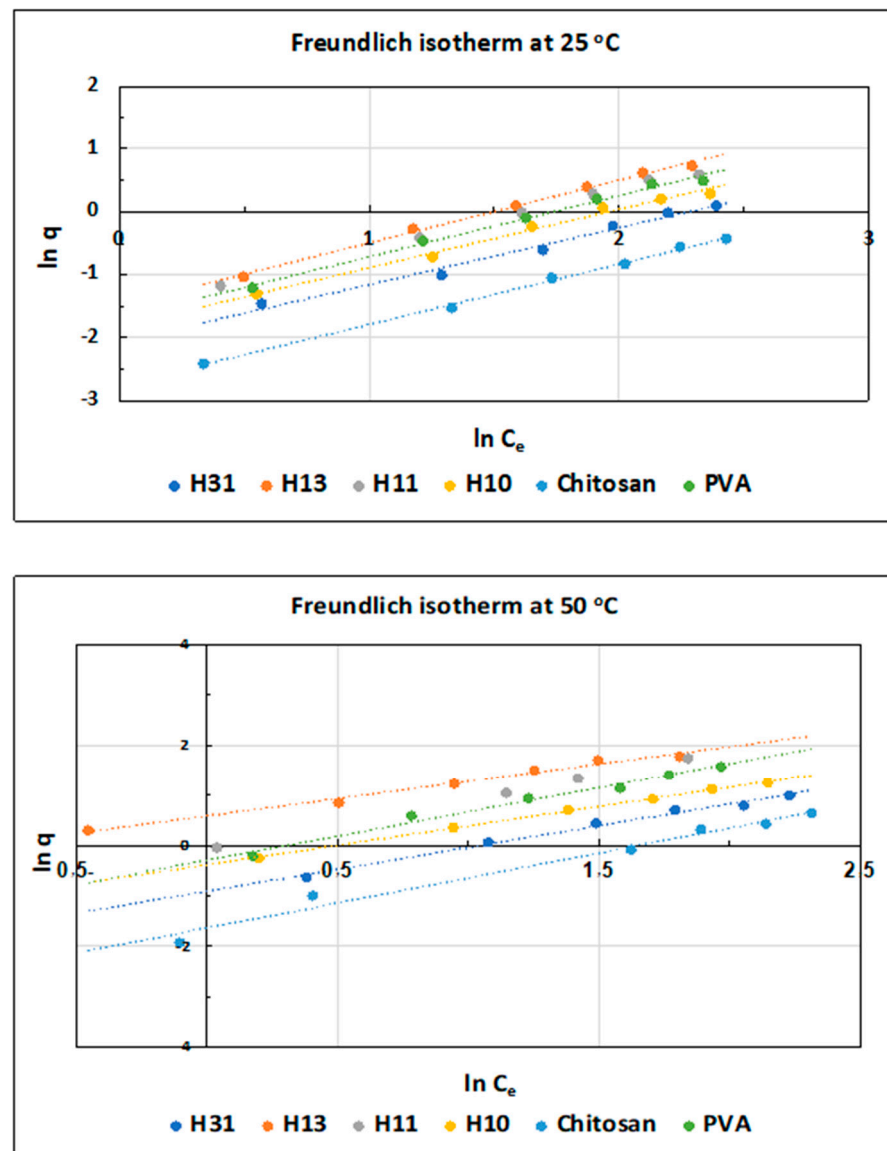


Figure 7. Freundlich isotherm of CV dye adsorption onto the prepared hydrogels.

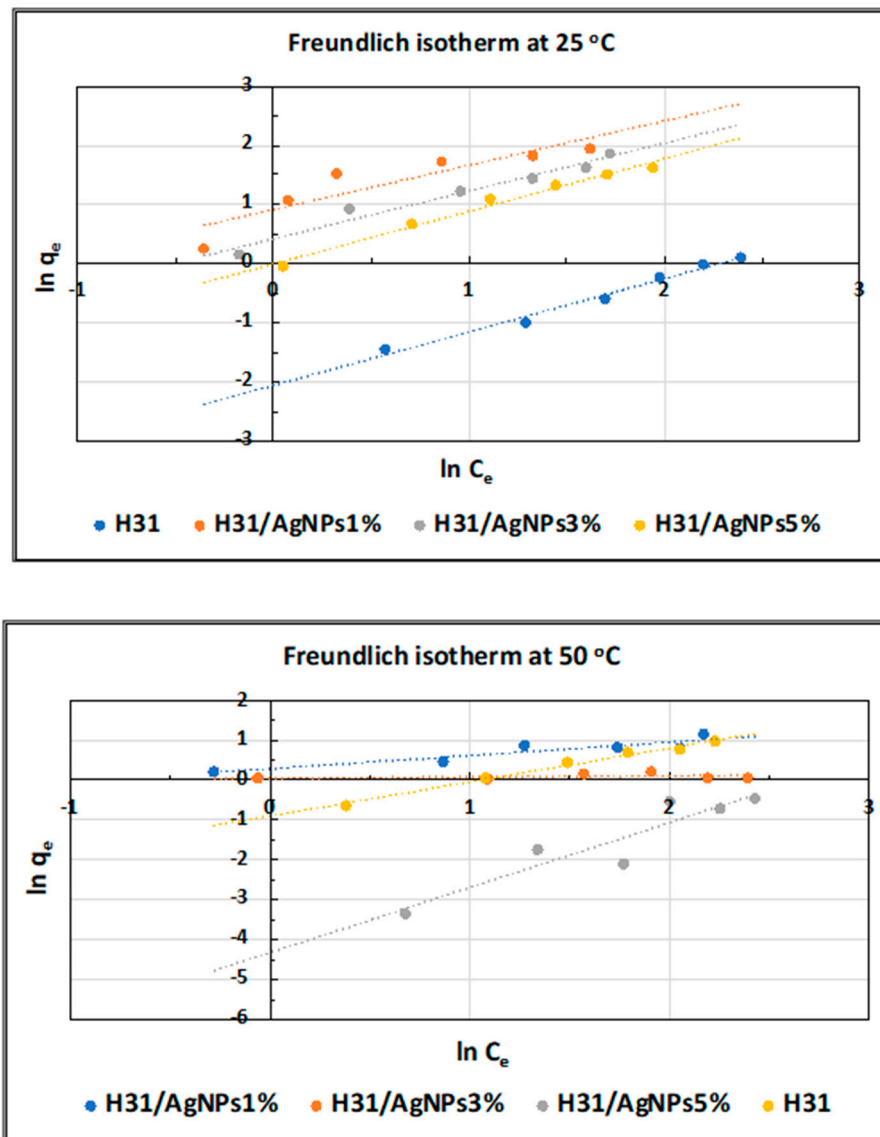


Figure 8. Freundlich isotherm of CV dye adsorption onto the H<sub>31</sub> and the H<sub>31</sub>/AgNP composites.

Table 3. Isotherm parameters obtained from Langmuir equation for the adsorption of the CV dye onto the prepared hydrogels and the H<sub>31</sub>/AgNP composites at 25 and 50 °C.

Temperature	Parameter	PVA	Chitosan	H <sub>10</sub>	H <sub>11</sub>	H <sub>13</sub>	H <sub>31</sub>	H <sub>31</sub> /AgNPs1%	H <sub>31</sub> /AgNPs3%	H <sub>31</sub> /AgNPs5%
25 °C	$q_{max}$ (mg g <sup>-1</sup> )	19.92	8.547	8.17	15.87	50.505	7.994	-9.804	-11.111	-21.277
	$K_L$ (L mg <sup>-1</sup> )	0.009	0.007	0.02	0.013	0.0046	0.015	-26.422	-18.044	-21.979
	R <sup>2</sup>	0.216	0.324	0.474	0.578	0.132	0.22	0.088	0.462	0.524
	R <sub>L</sub>	0.981–0.898	0.985–0.919	0.962–0.808	0.974–0.861	0.991–0.948	0.971–0.849	-0.019–0.003	-0.02–0.005	-0.023–0.004
50 °C	$q_{max}$ (mg g <sup>-1</sup> )	43.48	52.63	8.547	322.6	11.364	9.009	-1.828	-0.859	12.987
	$K_L$ (L mg <sup>-1</sup> )	0.018	0.004	0.079	0.003	0.1833	0.046	-3.435	-1.408	0.247
	R <sup>2</sup>	0.178	0.010	0.872	0.215	0.891	0.853	0.558	0.067	0.757
	R <sub>L</sub>	0.966–0.826	0.993–0.957	0.863–0.513	0.994–0.967	0.732–0.313	0.915–0.643	-0.170–0.025	-0.551–0.063	0.670–0.252

**Table 4.** Isotherm parameters obtained from Freundlich equation for the adsorption of the CV dye onto the prepared hydrogels and the H<sub>31</sub>/AgNP composites at 25 and 50 °C.

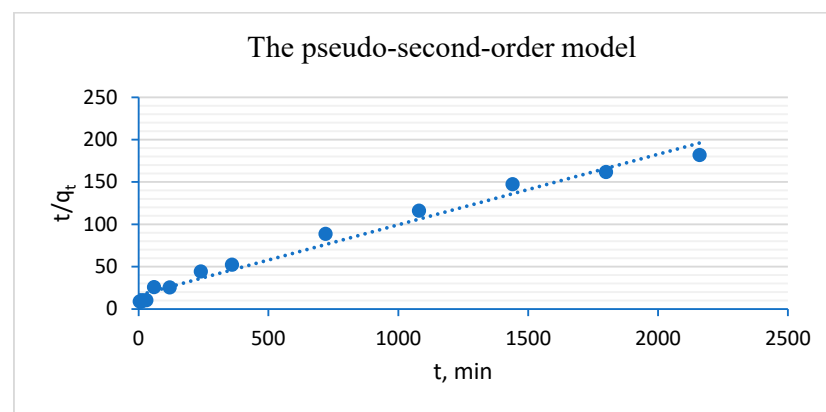
Temperature	Parameter	PVA	Chitosan	H <sub>10</sub>	H <sub>11</sub>	H <sub>13</sub>	H <sub>31</sub>	H <sub>31</sub> /AgNPs1%	H <sub>31</sub> /AgNPs3%	H <sub>31</sub> /AgNPs5%
25 °C	1/n	0.974	0.962	0.925	0.951	0.992	0.90	1.084	1.192	1.105
	$K_f$ (mg g <sup>-1</sup> ) (L mg <sup>-1</sup> )	0.186	0.064	0.164	0.213	0.228	0.129	0.418	0.629	1.022
	R <sup>2</sup>	0.992	0.997	0.989	0.997	0.997	0.983	0.815	0.963	0.981
50 °C	1/n	0.95	0.992	0.78	0.993	0.69	0.86	2.505	2.787	0.529
	$K_f$ (mg g <sup>-1</sup> ) (L mg <sup>-1</sup> )	0.752	0.195	0.68	0.924	0.5532	0.409	0.587	3.469	12.528
	R <sup>2</sup>	0.893	0.98	0.998	0.999	0.985	0.99	0.830	0.857	0.863

### 2.3. Adsorption Kinetics

The kinetic outcomes of the adsorption of CR dye by H<sub>31</sub> and that of CV dye by H<sub>13</sub> are listed in Table 5. The adsorption plots of the pseudo-first order and the pseudo-second order are illustrated in online Supplemental Files S5 and S6 and Figures 9 and 10, respectively.

**Table 5.** The kinetic model constants and the correlation coefficients for the adsorption of the CR and CV dyes onto the hydrogels.

Kinetic Models	Parameters	CR	CV
		H <sub>31</sub>	H <sub>13</sub>
pseudo-first-order	$q_{e,exp}$ (mg g <sup>-1</sup> )	13.45	1.67
	R <sup>2</sup>	0.970	0.959
	$q_{e,cal}$ (mg g <sup>-1</sup> )	11.05	1.34
	$K_1$ (10 <sup>-4</sup> ) (min <sup>-1</sup> )	1.74	1.74
	$\Delta q_e$ (%)	5.15	5.70
pseudo-second-order	R <sup>2</sup>	0.980	0.990
	$q_{e,cal}$ (mg g <sup>-1</sup> )	12.00	1.67
	$K_2$ (10 <sup>-4</sup> ) (g·mg <sup>-1</sup> ·min <sup>-1</sup> )	4.28	45.77
	$\Delta q_e$ (%)	3.11	0

**Figure 9.** A plot of linear regressions of the pseudo-second-order kinetic model for the adsorption of CR dye onto H<sub>31</sub>.

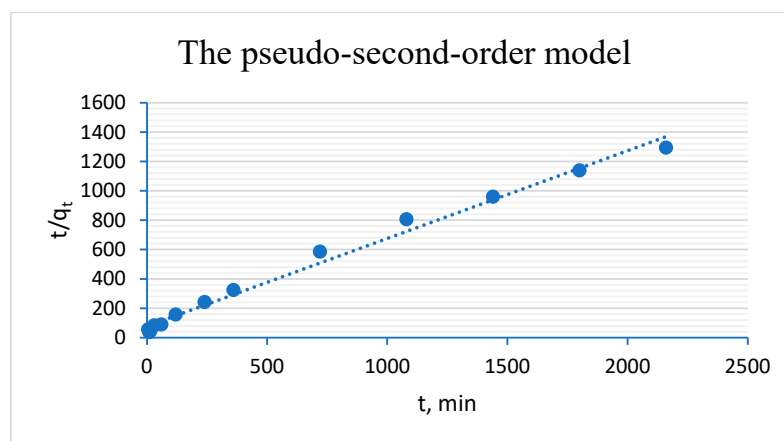


**Figure 10.** A plot of the linear regressions of the pseudo-second-order kinetic model for the adsorption of CV dye onto H<sub>13</sub>.

The pseudo-second-order model showed a higher value of correlation coefficients,  $R^2$ , (0.980 for H<sub>31</sub> and 0.990 for H<sub>13</sub>) than did the pseudo-first order model (0.970 for H<sub>31</sub> and 0.959 for H<sub>13</sub>). This is owed to the fact that the pseudo-second-order model shows a typical fit for describing the adsorption of both CR and the CV dyes onto the H<sub>31</sub> and the H<sub>13</sub> surfaces. In addition, there is good consistence between the values of the experimental and calculated  $q_e$  for the pseudo-second-order model, which are equal to 13.45 and 12.00 mg g<sup>-1</sup>, respectively, for the adsorption of CR onto H<sub>31</sub>, and are equal to 1.67 and 1.67 mg g<sup>-1</sup>, respectively, for the adsorption of CV dye onto H<sub>13</sub>. This indicates and emphasizes the outstanding fit of the pseudo-second-order kinetic model for the adsorption of CR and CV dyes by H<sub>31</sub> and H<sub>13</sub>, respectively.

#### 2.4. Desorption Studies

The ability to reuse adsorbents is deemed to be one of the most significant characteristics that reduces the costs of adsorption techniques via the renewal of adsorbents [12].

The desorption of the CR and the CV dyes was calculated using Equation (14). Methanol, as a desorption medium, showed that the desorption percentage reached 75 and 79% for the adsorption of CR and CV dyes onto H<sub>31</sub>, respectively, and reached 65 and 73% for the adsorption of CR and CV onto H<sub>13</sub>, respectively (Figure 11). These outcomes proved that the hydrogels could be effectively reused to adsorb both the CR and the CV dyes from their aqueous solutions.

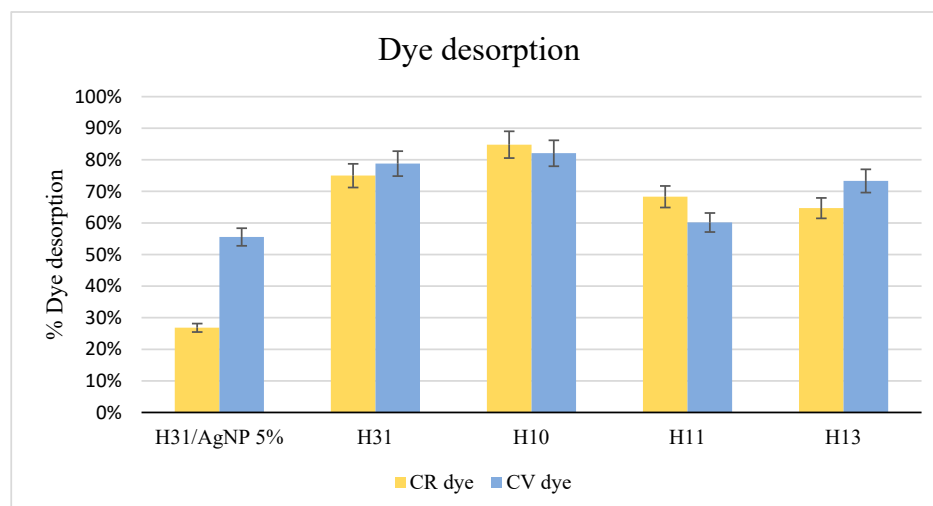


**Figure 11.** Desorption percentages of CR and the CV dyes from the adsorbents.

### 2.5. Comparison of Sorption Capacity for CR and CV Dyes onto Various Adsorbents

To identify the performance of the synthesized hydrogels and the H<sub>31</sub>/AgNP composites, in the present study, their maximum adsorption capacities for both the CR and CV dyes were compared with those of other adsorbents, as shown in Tables 6 and 7, respectively. The investigated hydrogels and the H<sub>31</sub>/AgNPs5% composite showed an adsorption capacity for CR dye that was better than that of some of the reported adsorbents [33,38–42], and that was lower than that of others [43–46] listed in Table 6. This reflects the prospects of boosting the adsorption capacity of PVA for CR dye via blending it with cross-linked chitosan and dispersing AgNPs into its matrices. This is due to the incorporation of a variety of cationized functional moieties during the cross-linking process which act as sites for binding the anionic CR dye. Thus, it is concluded that the synthesized hydrogels and the H<sub>31</sub>/AgNP composites can be considered favorable adsorbents for CR dye removal. On the other hand, in the case of CV dye, the adsorption capacity of the synthesized hydrogels and the H<sub>31</sub>/AgNPs5% composite was less than that of the previously reported adsorbents (Table 7) [47–53].

**Table 6.** Performance characteristics of some adsorbents for the removal of CR dye.

Adsorbents	Adsorption Capacity, $q_{max}$ (mg/g)	pH	Initial Dye Concentration (mg/L)	Dosage of Adsorbent	References
Zeolite (clay materials)	3.77	7.5 ± 0.3	150.0	100 g/L	[38]
ZrO <sub>2</sub> reagent	4.8 ± 0.2	7.0	35.0	400 mg/L	[33]
Natural kaolin (K)	5.94	6.9	100.0	0.1 g/10 mL	[39]
Australian kaolin clay K15GR	6.81	7.5 ± 0.3	200.0	50.0 g/L	[40]
Australian kaolin clay Ceram	7.27	7.5 ± 0.3	250.0	20.0 g/L	[40]
Nickel oxide nanoparticles	10.10	5.0	2.0	0.5 g/L	[41]
Montmorillonite	12.70	7.0	100	0.1 g/25 mL	[42]
H <sub>13</sub>	13.78	7	18	0.01 g/10 mL	This work
H <sub>11</sub>	16.247	7	18	0.01 g/10 mL	This work
H <sub>31</sub>	17.93	7	18	0.01 g/10 mL	This work
H <sub>31</sub> /AgNPs 5%	17.98	7	18	0.01 g/10 mL	This work
Polypyrrole	18.00	3.0	40.0	100 mg/50 mL	[43]
Raw rectorite (R-REC)	19.50	7.0	500.0	0.025 g/25 mL	[44]
ZrO <sub>2</sub> solid spheres	21.4 ± 1.1	7.0	35.0	400 mg/L	[33]
Open burnt clay	22.86	3.0	50.0	0.5 g/200 mL	[45]
Cetyltrimethylammonium bromide-modified kaolin (CTAB-kaolin or KC)	24.46	6.9	100.0	0.1 g/10 mL	[39]
Raw clay	27.03	7.5 ± 0.2	50.0	1.0 g/100 mL	[46]

**Table 7.** Performance characteristics of some adsorbents for the removal of CV dye.

Adsorbent	$q_{max}$ (mg/g)	$C_o$ (mg/L)	pH	References
H <sub>31</sub>	2.7	12	7	This work
H <sub>11</sub>	5.7	12	7	This work
H <sub>13</sub>	5.89	12	7	This work
H <sub>31</sub> /AgNPs 5%	11.365	12	7	This work

Table 7. Cont.

Adsorbent	$q_{max}$ (mg/g)	$C_o$ (mg/L)	pH	References
Eichhornia crassipes live roots	20.84	1000	7	[47]
Jackfruit leaf powder (JLP)	43.39	100	7	[48]
NaOH-modified rice husk (NMRH)	44.87	50	8	[49]
Banyan leaf powder	81	150	8	[50]
Grapefruit peel	249.68	100	6	[51]
Treated ginger waste (TGW)	277.7	20	8	[52]
NaOH-activated Aerva javanica leaf (NAJL)	315.2	250	9	[53]

### 3. Conclusions

The adsorption capacity and the % removal efficiency for CR dye of the investigated hydrogels and the H<sub>31</sub>/AgNP composites increased with the increase in their H<sub>10</sub> and AgNP content, and can be arranged as follows: H<sub>31</sub>/AgNPs5% > H<sub>31</sub>/AgNPs3% > H<sub>31</sub>/AgNPs1% > H<sub>31</sub> > H<sub>10</sub> > H<sub>11</sub> > chitosan > H<sub>13</sub> > PVA. This is due to the increased number of incorporated thiourea and amide moieties in chitosan after the cross-linking process, from H<sub>13</sub> to H<sub>31</sub>, which work as efficient binding sites for CR anionic dye via electrostatic interaction and hydrogen bond formation. Contrary to the results for the CR anionic dye, the capacity for the CV cationic dye to adsorb onto the prepared hydrogels and the H<sub>31</sub>/AgNP composites can be classified as follows: H<sub>31</sub>/AgNPs5% > H<sub>31</sub>/AgNPs3% > H<sub>31</sub>/AgNPs1% > H<sub>13</sub> > H<sub>11</sub> > PVA > H<sub>10</sub> > H<sub>31</sub> > chitosan. Thus, the adsorption capacity and the removal efficiency for CV dye of the prepared hydrogels increased with an increase in their PVA content, i.e., from H<sub>31</sub> to H<sub>13</sub>. Further, the loading of silver nanoparticles inside the H<sub>31</sub> matrices enhanced the adsorption efficiencies of the resulting composites in comparison to those of the H<sub>31</sub> due to the increased surface area, in addition to the many cross-linkages that originated between the AgNPs and the electron-rich nitrogen and oxygen atoms of the components of the hydrogels. The adsorption capacity for both the CR and the CV dyes of the prepared hydrogels and the H<sub>31</sub>/AgNP composites is greatly dependent on the initial dye concentration, the temperature, and the initial pH of the dye solution. The adsorption kinetics were effectively explained using a pseudo-second-order model for both the dyes. The Freundlich isotherm model fitted better to the experimental results of the adsorption of the CV dye onto the prepared hydrogels and the H<sub>31</sub>/AgNP composites, indicating that multilayer adsorption occurred on the heterogeneous surfaces. Thus, one can conclude that the incorporation of PVA, H<sub>10</sub>, and AgNPs in the same hydrogel matrix considerably enhances the PVA adsorption capacity for CR and the CV dyes, depending on the content of both H<sub>10</sub> and the AgNPs in the hydrogel. Thus, it is possible to synthesize PVA hydrogels with good adsorption capabilities for cationic and anionic dyes via the adjustment of the H<sub>10</sub> and AgNP content in these hydrogels. This is a suitable approach with which to attain promising materials that can efficiently compete with traditional adsorbents.

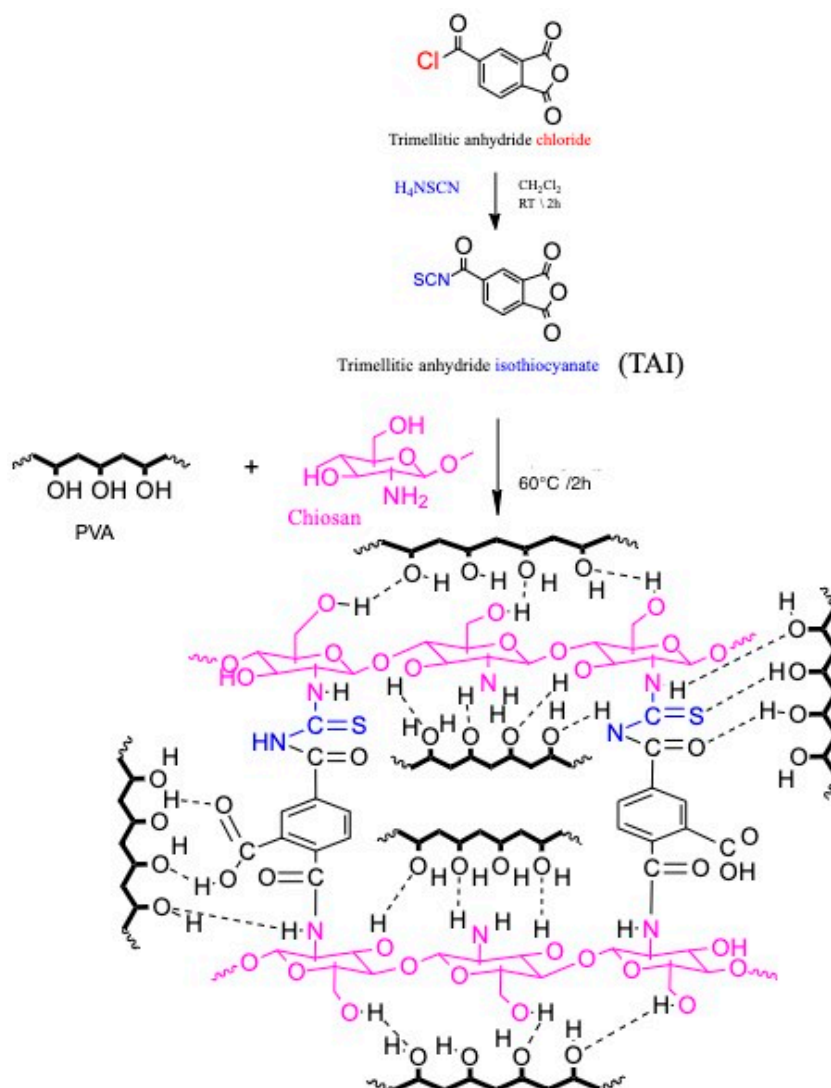
### 4. Materials and Methods

#### 4.1. Materials

Chitosan, with a deacetylation degree of 88.2% and a molecular mass of  $2.9\text{--}3.1 \times 10^5$  g mol<sup>-1</sup>, was supplied by Funakoshi Co. Ltd., (Tokyo, Japan). Ammonium thiocyanate (99.99%), silver nitrate (>99%), polyethylene glycol-400, trisodium citrate ( $\geq 99\%$ ), and poly (vinyl alcohol), PVA, with a degree of hydrolysis of 99.0–99.8% and molecular mass of  $8.9\text{--}9.8 \times 10^4$  g mol<sup>-1</sup>, were purchased from Sigma-Aldrich (Saint Louis, MO, USA). Trimellitic anhydride chloride (98%) was provided by Aldrich (Darmstadt, Germany). Congo Red (CR,  $\geq 98$ ,  $\lambda_{max} = 497$  nm) and Crystal Violet (CV,  $\geq 98$ ,  $\lambda_{max} = 600$  nm) dyes were obtained from Winlab (Leicestershire, UK). Online Supplemental File S7 shows the chemical structure of both the dyes, and their calibration curves.

#### 4.2. Preparation of Chitosan/PVA Hydrogels

Following the procedure reported in our previous work [25], firstly, a prespecified molar quantity of solid trimellitic anhydride chloride was gradually added to an equimolar quantity of  $\text{NH}_4\text{SCN}$  that was dissolved in 25 mL of  $\text{CH}_2\text{Cl}_2$ , followed by the addition of polyethylene glycol-400 (1 mL), a phase transfer agent, stirring this well at 25 °C for 120 min. The reaction mixture was filtered to isolate the white precipitate (the by-product,  $\text{NH}_4\text{Cl}$ ) and obtain the trimellitic anhydride isothiocyanate cross-linker (TAI, Scheme 3) as a filtrate [25]. Secondly, a chitosan solution (1.5% wt/v using aqueous acetic acid (1% v/v) as a solvent) was blended with a PVA solution (5.0% wt/v, in distilled water at 60 °C), stirring this well at 60 °C for 60 min. TAI was slowly added to the resulting chitosan/PVA blend solutions with various weight ratios (Table 8), stirring this well at 60 °C for 120 min, and then at room temperature overnight. The molar ratio of TAI to the chitosan component in the blend was 1:2, respectively (Table 8 and Scheme 3). The acetic acid was eliminated from the resulting hydrogels via a neutralizing reaction using a  $\text{NaHCO}_3$  solution, then soaked in methanol for dewatering and desalting, filtration, and finally drying at 60 °C. The obtained hydrogels showed a color ranging from faint yellow to dark yellow in accordance with the TAI content that was based on the content of chitosan in the hydrogel. The ratios of the reactants are summarized in Table 8, with the production of four hydrogels symbolized as  $\text{H}_{10}$ ,  $\text{H}_{11}$ ,  $\text{H}_{13}$ , and  $\text{H}_{31}$  [25].



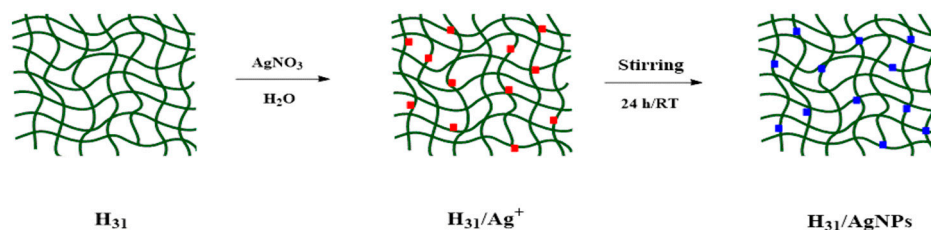
Scheme 3. PVA/chitosan blend-based hydrogels.

**Table 8.** Synthesis and elemental analyses of the prepared hydrogels.

Hydrogel Code	Chitosan: PVA (Weight Ratio)	Chitosan g (mmol)	PVA (g)	Trimellitic Anhydride Chloride g (mmol)	Ammonium Thiocyanate g (mmol)	Elemental Analysis (%)				
						C	H	N	O	S
Chitosan	-	-	-	-	-	45.10	6.77	8.43	39.70	-
PVA	-	-	-	-	-	54.54	9.10	-	36.36	-
H <sub>10</sub>	1:0	3 (18.63)	0	1.96 (9.32)	0.71 (9.32)	47.54	4.68	7.51	35.03	5.24
H <sub>13</sub>	1:3	1 (6.21)	3	0.65 (3.11)	0.24 (3.11)	52.79	8.00	1.88	36.02	1.31
H <sub>11</sub>	1:1	2 (12.42)	2	1.31 (6.21)	0.47 (6.21)	51.04	6.89	3.75	35.70	2.62
H <sub>31</sub>	3:1	3 (18.63)	1	1.96 (9.32)	0.71 (9.32)	49.29	5.79	5.63	35.36	3.93

#### 4.3. Preparation of H<sub>31</sub>/Silver Nanoparticle (H<sub>31</sub>/AgNP) Composites

Three different predetermined quantities of AgNO<sub>3</sub> were separately dissolved in 10 mL of deionized H<sub>2</sub>O. Each AgNO<sub>3</sub> solution was stirred with a constant weight of H<sub>31</sub> (1 g) that priorly swelled in 50 mL of trisodium citrate solution (0.01 mol L<sup>-1</sup>) at room temperature for 24 h. A perceivable color variation in the three producing composites was detected that ranged from light to dark brown in proportion to the increase in the AgNO<sub>3</sub> concentration. This indicated that the Ag<sup>+</sup> cations were reduced to AgNPs inside the H<sub>31</sub> matrix (Scheme 4). The composites were filtered, rinsed repeatedly with water then methanol, and dried at 60 °C. The used concentrations of silver nitrate were 1 wt%, 3 wt%, and 5 wt% in accordance with the weight of H<sub>31</sub>, producing three composites symbolized as H<sub>31</sub>/AgNPs1%, H<sub>31</sub>/AgNPs3%, and H<sub>31</sub>/AgNPs5%, respectively [25].

**Scheme 4.** Synthesis of H<sub>31</sub>/AgNP composite.

#### 4.4. Characterization of Chitosan/PVA Hydrogels and H<sub>31</sub>/AgNP Composites

The structure and morphology of the prepared hydrogels and H<sub>31</sub>/AgNP composites were confirmed using various analytical techniques: elemental (Perkin Elmer C, H, N, S Analyzer, Model 2410 series II, Waltham, MA, USA), FTIR (Agilent Technologies FTIR Spectrometer, Cary 600 Series, Santa Clara, CA, USA), XPS (Kratos XSAM Spectrometer, Model 800, Manchester, UK), XRD (advanced wide-angle X-ray diffractometer (Bruker's D-8), SEM (scanning electron microscope, Jeol-JSM-6060LV), EDS (scanning electron microscope (Quanta FEG 250) equipped with an energy-dispersive X-ray spectrometer) and TEM (transmission electron microscope (JEM-HR-JEOL-JEM2100) analyses. The results, shown in online Supplemental File S8, were well in agreement with those reported in our previous work [25].

Table 8 illustrates that the percentage of nitrogen and sulfur increased with increasing H<sub>10</sub> content in the hydrogels (from H<sub>13</sub> to H<sub>31</sub>), while the percent of carbon, hydrogen, and oxygen increased with the increasing PVA content in the hydrogels (from H<sub>31</sub> to H<sub>13</sub>), indicating the successful preparation of chitosan/PVA hydrogels.

In comparison to the FTIR spectra of chitosan and PVA, shown in online Supplemental File-S8 (1), all the prepared hydrogels showed similar spectra that were characterized by the disappearance of the doublet peak of the primary amine groups of chitosan, and the appearance of a new peak around 1717 cm<sup>-1</sup> attributed to **COOH** in the cross-linking linkages. The peak of **COOH** in the cross-linking linkages overlapped with that of the NH groups. The overlap between the peaks of the **-CONH**, NH (secondary amide), and

aromatic C=C bonds resulted in the appearance of a new peak near  $1656\text{ cm}^{-1}$ . The peak of the C=S groups that overlapped with the stretching vibration of C-O appeared as a strong broad peak around  $1085\text{ cm}^{-1}$ . The bending vibration peaks of N-C-S groups were observed near  $1424$  and  $588\text{ cm}^{-1}$ . The intensity of these peaks increased with an increasing cross-linker linkage content and consequently with the increasing chitosan content in the prepared hydrogels, i.e., from H<sub>13</sub> to H<sub>31</sub>. Moreover, the FTIR spectra of H<sub>31</sub>/AgNPs3% and H<sub>31</sub>/AgNPs5%, shown in online Supplemental File S8 (2), displayed additional peaks in the range of  $500\text{--}800\text{ cm}^{-1}$ , indicating AgNP formation inside the composites.

The XPS spectrum of the H<sub>31</sub>/AgNPs5% composite, shown in online Supplemental File S8 (3), proves the formation of AgNPs. It shows two peaks at 368.2 and 374.0 eV which are consistent with 3d<sub>5/2</sub> and 3d<sub>3/2</sub> for silver metal. The other two peaks at 370.3 and 376.1 eV could be attributed to the complex resulting from the interaction of silver with the carbonyl and hydroxyl groups in H<sub>31</sub>.

Compared to the XRD pattern of virgin chitosan, shown in online Supplemental File S8 (4), which exhibited two peaks around  $2\theta = 10^\circ$  and  $20^\circ$ , corresponding to its amorphous and crystalline fractions, respectively, that of H<sub>10</sub> showed an increase in its amorphous fraction and a decrease in its crystalline fraction. This is due to the consumption of the hydrogen bond-forming functional groups during the cross-linking process. Virgin PVA showed three peaks: around  $2\theta = 10^\circ$  (very weak and broad), near  $2\theta = 20^\circ$  (very intensive and sharp), and around  $2\theta = 40^\circ$  (weak and broad). H<sub>13</sub>, H<sub>11</sub>, and H<sub>31</sub> displayed three relatively amorphous peaks around  $2\theta = 10^\circ$ ,  $20^\circ$ , and  $40^\circ$ . Their intensities and sharpness increased with an increase in the PVA proportion in the hydrogels (from H<sub>31</sub> to H<sub>13</sub>).

The generation of AgNPs in the matrices of H<sub>31</sub>, as shown in online Supplemental File S8 (5), was confirmed via XRD analysis, which showed some characteristic crystalline peaks near  $2\theta$   $38.18^\circ$ ,  $44.25^\circ$ ,  $64.55^\circ$ ,  $77.58^\circ$ , and  $81.81^\circ$  with plane distances of 2.357 Å, 2.039 Å, 1.444 Å, 1.229 Å, and 1.165 Å, respectively, which are consistent with those of the pure Ag metal. Their intensity increased with an increase in the AgNP content in H<sub>31</sub>. These peaks were indexed to the crystal planes of (111), (200), (220), (311), and (222) of face-centered cubic (fcc) Ag.

SEM images of chitosan and PVA, shown in online Supplemental File S8 (6), showed smooth surfaces, while all the prepared hydrogels had rough surfaces full of grooves and containing a lot of homogeneously distributed pores resulting from the cross-linking process, resulting in very open structures with increased surface areas. These pores facilitated the penetration of water into the hydrogel and acted as sites of interaction between the external stimuli and the hydrophilic polar groups of the hydrogels. The pores were denser and more regular with an increasing H<sub>10</sub> content in the hydrogel due to the increased concentration of the used cross-linker.

The in situ-created AgNPs were homogeneously distributed without agglomeration or aggregation as bright spots into H<sub>31</sub>/AgNP composites, as shown via the SEM images in online Supplemental File S8 (7). This is owed to the existence of a lot of marked capping groups on H<sub>31</sub>, acting as efficient ligands for the stabilization of the formed AgNPs. Moreover, the EDS diagram of H<sub>31</sub>/AgNPs3% showed a peak corresponding to that of silver of 5.98 wt%, indicating the considerable adsorption of AgNPs onto H<sub>31</sub>.

TEM images of H<sub>31</sub>/AgNPs5% composites at different magnifications, shown in online Supplemental File S8 (8), illustrated the uniform dispersion of the AgNPs as spherically shaped spots of sizes ranging between 13 and 26 nm.

#### 4.5. pH of Zero-Point Charge—pHzpc

The pH<sub>zpc</sub> is a significant parameter that enables thorough comprehension of surface adsorption mechanisms. To determine the pH<sub>zpc</sub>, 10 mg of the hydrogel was stirred overnight in 10 mL of the NaCl solutions (0.01 M) at initial assorted pH values varying between 2 and 10. The pH values of these solutions were adjusted utilizing HCl/NaOH solutions (0.1 M). The pH<sub>zpc</sub> is determined as the pH value at  $\Delta\text{pH} = 0$  [24].

#### 4.6. Batch Adsorption Tests

Congo Red (CR) and Crystal Violet (CV) dyes were selected in this study as representative examples for the anionic and the cationic dyes, respectively, due to their large-scale use in various dyeing processes.

A series of batch tests proceeded for determining the adsorption capability of both CR and CV dyes onto the prepared hydrogels and H<sub>31</sub>/AgNP composite adsorbents. The experiment on dye adsorption was carried out using 10 mg of the adsorbent in 10 mL of an aqueous dye solution of concentrations ranging from 2 to 18 mg L<sup>-1</sup>, at 25 and 50 °C, at pH 4, 7, and 9, and under a shaking speed of 80 rpm for 48 h, at which point an equilibrium in all the measurements was attained. HCl and NaOH were used to adjust the pH of the dye solutions. The unabsorbed portion of the dyes in the solution was spectrometrically determined using a Shimadzu UV/Vis 1650 spectrophotometer at 497 nm for CR dye and at 600 nm for CV dye.

The adsorption capacity and the % removal efficiency of the adsorbent for the dyes were calculated based on Equations (1)–(3) [12]:

$$q_e = \frac{(C_o - C_e)xV}{W} \quad (1)$$

$$q_t = \frac{(C_o - C_t)xV}{W} \quad (2)$$

$$\% \text{ Removal efficiency} = \left( \frac{(C_o - C_e)}{C_o} \right) \times 100 \quad (3)$$

where  $q_e$  and  $q_t$  (mg g<sup>-1</sup>) are the amount of the adsorbed dye at the equilibrium time and  $t$  time, respectively,  $C_o$  (mg L<sup>-1</sup>) is the initial concentration of the dye,  $C_e$  (mg L<sup>-1</sup>) is the concentration of the dye at the equilibrium time,  $V$  (L) is the volume of the dye solution, and  $W$  (g) is the weight of the adsorbent.

#### 4.7. Adsorption Isotherms

The adsorption isotherm indicates the relation that associates the quantity of the solute adsorbed by the adsorbent and the solute concentration in the solution at the equilibrium at a certain temperature.

##### Types of Adsorption Isotherm Equations

In the last decade, several equilibrium isotherm models have been established, such as the Brunauer-Emmett-Teller, Dubinin-Radushkevich, Koble-Corrigan, Flory-Huggins, Redlich-Peterson, Radke-Prausnitz, Khan, Temkin, Toth, Hill, Sips, Langmuir, and Freundlich isotherm models. These models were derived in accordance with three essential advances: (i) kinetic considerations where the rates of adsorption and desorption are similar, (ii) the thermodynamic basis, and (iii) the potential theory that commonly communicates a major idea in the plotting of characteristic curves [54–56].

There are several models that are used for determining equilibrium distribution, but for the treatment of wastewater, the most commonly used models are the Freundlich and Langmuir isotherm models [54,56,57].

##### ❖ Langmuir isotherm equation

The theory of Langmuir adsorption correlates the rapid lowering of attraction forces with the increase in distance between the molecules. This model has two parameters, as illustrated via Equation (4):

$$q_e = \frac{q_{max}K_L C_e}{1 + K_L C_e} \quad (4)$$

Equation (4) can be transformed into a linearized form, Equation (5):

$$\frac{C_e}{q_e} = \frac{1}{K_L q_{max}} + \frac{C_e}{q_{max}} \quad (5)$$

where  $q_{max}$  is the maximum adsorption capacity for forming a monolayer ( $\text{mg g}^{-1}$ ) and  $K_L$  is the Langmuir constant ( $\text{L mg}^{-1}$ ).

From the Langmuir linear equation,  $K_L$  and the  $q_{max}$  were obtained from the intercept and the slope of the linearized plot of  $C_e/q_e$  against  $C_e$ . For the description of the isotherm type, the dimensionless constant (the separation factor or the equilibrium parameter) ( $R_L$ ) could be determined by applying Equation (6):

$$R_L = \frac{1}{1 + K_L C_0} \quad (6)$$

where  $R_L$  shows the nature of sorption to be either unfavorable for  $R_L > 1$ , linear for  $R_L = 1$ , favorable for  $0 < R_L < 1$ , or irreversible for  $R_L = 0$  [55,58].

#### ❖ Freundlich isotherm equation

The Freundlich isotherm is the first formula that demonstrates reversible and non-ideal sorption, sorption which is not adequate for monolayer formation. It has two parameters, as indicated in Equation (7):

$$q_e = K_f C_e^{\frac{1}{n}} \quad (7)$$

where  $K_f$  is the Freundlich constant ( $\text{mg g}^{-1}$ ) ( $\text{L mg}^{-1}$ ) and  $n$  is the adsorption intensity.

Equation (7) can be transformed into a linearized form, Equation (8):

$$\ln q_e = \ln K_f + \left(\frac{1}{n}\right) \ln C_e \quad (8)$$

The values of  $1/n$  and  $K_f$  were obtained by plotting  $\ln q_e$  against  $\ln C_e$  as the slope and the intercept, respectively. Briefly,  $1/n$  (the intensity of the adsorption) predicts any phenomenon that happens along the process of adsorption;  $1/n < 1$  means normal adsorption;  $1/n > 1$  means cooperative adsorption; and  $1/n$  being near to zero means that the adsorbent surface is more heterogeneous [58].

#### 4.8. Adsorption Kinetics

Exploring the adsorption kinetics is also useful for grasping the rate of adsorption on the adsorbent surface, because the adsorption kinetics exhibit the impact of the diverse conditions on the adsorption process' quickness, applying models which describe the adsorption reaction. Moreover, the adsorption kinetics provide the mechanism of adsorption of the dyes by the adsorbents.

The kinetic outcomes for the two investigated dyes (CR and CV) were modeled by employing two various kinetic models: pseudo-first-order, and pseudo-second-order models.

#### ❖ Pseudo-First-Order Model (Lagergren Model)

This model is used to determine the relation between alterations in time and the capability of adsorption with an order of one. It is given via Equation (9), where  $k_1$  is the rate constant:

$$\frac{q_t}{t} = k_1 (q_e - q_t) \quad (9)$$

Integrating Equation (9) with the boundary conditions of  $q_t = 0$  at  $t = 0$  and  $q_t = q_t$  at  $t = t$  gives a linear equation of the pseudo-first-order model, Equation (10):

$$\log(q_e - q_t) = \log q_e - \frac{k_1}{2.303} t \quad (10)$$

The values of  $q_e$  and  $k_1$  can be determined from the intercept and the slope of the linear plot of  $\log(q_e - q_t)$  versus  $t$ .

❖ Pseudo-Second-Order Model (Ho and Mckay Model)

This model is given via Equation (11), which illustrates the relation between the capacity of adsorption and the concentration with a second order. It depicts the adsorption of the dissolved dye ions through chemical sharing or an exchange of cations on the surface of the adsorbents. This refers to a chemical reaction that occurs in the process of adsorption.

$$\frac{q_t}{t} = k_2(q_e - q_t)^2 \quad (11)$$

The integration of Equation (11) provides the linearized form of the pseudo-second-order equation: Equation (12).

$$\frac{t}{q_t} = \frac{1}{k_2 q_e^2} + \frac{t}{q_e} \quad (12)$$

where  $k_2$  is the pseudo-second-order constant ( $\text{g mg}^{-1} \text{min}^{-1}$ ). The slope and intercept of the linear plot of  $t/q$  against  $t$  yielded the values of  $q_e$  and  $k_2$ , respectively.

#### 4.9. Kinetic Validation

For the determination of the most usable model to describe the process of adsorption, the normalized standard deviation ( $\Delta q_e$  (%)) is determined and applied, employing Equation (13):

$$\Delta q(\%) = 100 \times \sqrt{\frac{[(q_{t,exp} - q_{t,cal}) / q_{t,exp}]^2}{N - 1}} \quad (13)$$

where  $q_{t,exp}$  is the experimental adsorption capacity ( $\text{mg g}^{-1}$ ),  $q_{t,cal}$  is the calculated adsorption capacity for pseudo-first- and pseudo-second-order models ( $\text{mg g}^{-1}$ ), and  $N$  is the number of data points.

#### 4.10. Desorption Study

The dye was desorbed from the adsorbent, firstly by rinsing it using distilled water to remove any non-adsorbed dye. Secondly, 10 mg of the adsorbent was individually soaked in 10 mL of various desorption media (EtOH, MeOH, MeCOMe, and a 0.1 N solution of NaOH) at 25 °C overnight. The quantity of the dye desorbed from the adsorbent could be determined by employing Equation (14):

$$\% \text{ Dye desorption} = q_d / q_a \times 100 \quad (14)$$

where  $q_d$  is the amount of dye desorbed from the adsorbent surface ( $\text{mg g}^{-1}$ ) and  $q_a$  is the amount of dye adsorbed onto the adsorbent ( $\text{mg g}^{-1}$ ) [12].

**Supplementary Materials:** The following supporting information can be downloaded at: <https://www.mdpi.com/article/10.3390/gels9110882/s1>.

**Author Contributions:** Supervision, N.A.M. and F.M.A.; conceptualization, N.A.M., N.F.A.-H., F.M.A. and N.Y.E.; methodology, N.A.M., N.F.A.-H., F.M.A. and N.Y.E.; investigation, R.T.A.; formal analysis, N.A.M., N.F.A.-H., F.M.A. and N.Y.E.; writing—original draft, R.T.A.; review and editing, N.A.M., N.F.A.-H., F.M.A. and N.Y.E. All authors have read and agreed to the published version of the manuscript.

**Funding:** This research received no external funding.

**Institutional Review Board Statement:** Not applicable.

**Informed Consent Statement:** Not applicable.

**Data Availability Statement:** The data presented in this study are available on request from the corresponding authors.

**Conflicts of Interest:** The authors declare no conflict of interest.

## References

1. Chung, K.-T. Azo dyes and human health: A review. *J. Environ. Sci. Health C* **2016**, *34*, 233–261. [[CrossRef](#)]
2. Dos Santos, A.B.; Cervantes, F.J.; Van Lier, J.B. Review paper on current technologies for decolourisation of textile wastewaters: Perspectives for anaerobic biotechnology. *Bioresour. Technol.* **2007**, *98*, 2369–2385. [[CrossRef](#)]
3. Khan, M.D.; Singh, A.; Khan, M.Z.; Tabraiz, S.; Sheikh, J. Current perspectives, recent advancements, and efficiencies of various dye-containing wastewater treatment technologies. *J. Water Process Eng.* **2023**, *53*, 103579. [[CrossRef](#)]
4. Cardoso, J.C.; Bessegato, G.G.; Boldrin Zanoni, M.V. Efficiency comparison of ozonation, photolysis, photocatalysis and photo-electrocatalysis methods in real textile wastewater decolorization. *Water Res.* **2016**, *98*, 39–46. [[CrossRef](#)]
5. El-Harby, N.F.; Ibrahim, S.M.A.; Mohamed, N.A. Adsorption of Congo red dye onto antimicrobial terephthaloyl thiourea cross-linked chitosan. *Water Sci. Technol.* **2017**, *76*, 2719–2732. [[CrossRef](#)]
6. Nagarkar, R.; Patel, J. Polyvinyl Alcohol: A Comprehensive Study. *Acta Sci. Pharm. Sci.* **2019**, *3*, 34–44.
7. Baker, M.I.; Walsh, S.P.; Schwartz, Z.; Boyan, B.D. A review of polyvinyl alcohol and its uses in cartilage and orthopedic applications. *J. Biomed. Mater. Res. Part B* **2012**, *100B*, 1451–1457. [[CrossRef](#)]
8. Mok, C.F.; Ching, Y.C.; Muhamad, F.; Osman, N.A.A.; Hai, N.D.; Hassan, C.R.C. Adsorption of Dyes Using Poly(vinyl alcohol) (PVA) and PVA-Based Polymer Composite Adsorbents: A Review. *J. Polym. Environ.* **2020**, *28*, 775–793. [[CrossRef](#)]
9. Lin, W.; Kluzek, M.; Iuster, N.; Shimoni, E.; Kampf, N.; Goldberg, R.; Klein, J. Cartilage-inspired, lipid-based boundary-lubricated hydrogels. *Science* **2020**, *370*, 335–338. [[CrossRef](#)]
10. Zhu, Y.; Liu, J.; Guo, T.; Wang, J.J.; Tang, X.; Nicolosi, V. Multifunctional Ti<sub>3</sub>C<sub>2</sub>T<sub>x</sub> MXene Composite Hydrogels with Strain Sensitivity toward Absorption-Dominated Electromagnetic-Interference Shielding. *ACS Nano* **2021**, *15*, 1465–1474. [[CrossRef](#)]
11. Shariatinia, Z.; Jalali, A.M. Chitosan-based hydrogels: Preparation, properties and applications. *Int. J. Biol. Macromol.* **2018**, *115*, 194–220. [[CrossRef](#)] [[PubMed](#)]
12. Elmehbad, N.Y.; Mohamed, N.A.; Abd El-Ghany, N.A.; Abdel-Aziz, M.M. Evaluation of the in vitro anti-inflammatory and anti-Helicobacter pylori activities of chitosan-based biomaterials modified with copper oxide nanoparticles. *Int. J. Biol. Macromol.* **2023**, *253*, 127277. [[CrossRef](#)] [[PubMed](#)]
13. Elmehbad, N.Y.; Mohamed, N.A. Synthesis, characterization, and antimicrobial activity of novel N-acetyl, N'-chitosanacetohydrazide and its metal complexes. *Int. J. Polym. Mater. Polym. Biomater.* **2022**, *71*, 1369–1379. [[CrossRef](#)]
14. Mohamed, N.A.; Abd El-Ghany, N.A. Synthesis, characterization, and antimicrobial activity of carboxymethyl chitosan-graft-poly(N-acryloyl, N'-cyanoacetohydrazide) copolymers. *J. Carbohydr. Chem.* **2012**, *31*, 220–240. [[CrossRef](#)]
15. Mei, Y.; Runjun, S.; Yan, F.; Honghong, W.; Hao, D.; Chengkun, L. Preparation, characterization and kinetics study of chitosan/PVA electrospun nanofiber membranes for the adsorption of dye from water. *J. Polym. Eng.* **2019**, *39*, 459–471. [[CrossRef](#)]
16. Elmehbad, N.Y.; Mohamed, N.A.; Abd El-Ghany, N.A.; Abdel-Aziz, M.M. Reinforcement of the antimicrobial activity and biofilm inhibition of novel chitosan-based hydrogels utilizing zinc oxide nanoparticles. *Int. J. Biol. Macromol.* **2023**, *246*, 125582. [[CrossRef](#)]
17. Wegrzynowska-Drzymalska, K.; Grebicka, P.; Mlynarczyk, D.T.; Chelminiak-Dudkiewicz, D.; Kaczmarek, H.; Goslinski, T.; Ziegler-Borowska, M. Crosslinking of Chitosan with Dialdehyde Chitosan as a New Approach for Biomedical Applications. *Materials* **2020**, *13*, 3413. [[CrossRef](#)]
18. Alharbi, R.A.; Alminderej, F.M.; Al-harby, N.F.; Elmehbad, N.Y.; Mohamed, N.A. Preparation and characterization of a new bis-uracil chitosan-based hydrogel as efficient adsorbent for removal of anionic Congo red dye. *Polymers* **2023**, *15*, 1529. [[CrossRef](#)]
19. Shahverdi, F.; Barati, A.; Bayat, M. Effective Methylene Blue Removal from Aqueous Solutions using PVA/Chitosan Electrospun Nanofiber Modified with CeAlO<sub>3</sub> Nanoparticles. *J. Water Environ. Nanotechnol.* **2022**, *7*, 55–68. [[CrossRef](#)]
20. Perez-Calderon, J.; Marin-Silva, D.A.; Zaritzky, N.; Pinotti, A. Eco-friendly PVA-chitosan adsorbent films for the removal of azo dye Acid Orange 7: Physical cross-linking, adsorption process, and reuse of the material. *Adv. Ind. Eng. Polym. Res.* **2022**, *6*, 239–254. [[CrossRef](#)]
21. Mahmoodi, N.M.; Mokhtari-Shourijeh, Z. Preparation of PVA-chitosan blend nanofiber and its dye removal ability from colored wastewater. *Fibers Polym.* **2015**, *16*, 1861–1869. [[CrossRef](#)]
22. Mohamed, N.A.; Al-Harby, N.F.; Almarshed, M.S. Synthesis and characterization of novel trimellitic anhydride isothiocyanate-cross linked chitosan hydrogels modified with multi-walled carbon nanotubes for enhancement of antimicrobial. *Int. J. Biol. Macromol.* **2019**, *132*, 416–428. [[CrossRef](#)]
23. Mohamed, N.A.; Al-Harby, N.F.; Almarshed, M.S. Enhancement of adsorption of Congo red dye onto novel antimicrobial trimellitic anhydride isothiocyanate-cross-linked chitosan hydrogels. *Polym. Bull.* **2020**, *77*, 6135–6160. [[CrossRef](#)]
24. Al-Harby, N.F.; Almarshed, M.S.; Mohamed, N.A. Effect of single-walled carbon nanotubes on the adsorption of Basic Red 12 Dye by trimellitic anhydride isothiocyanate-crossLinked chitosan hydrogel. *Cellul. Chem. Technol.* **2023**, *57*, 445–458. [[CrossRef](#)]
25. Alfuraydi, R.T.; Alminderej, F.M.; Mohamed, N.A. Evaluation of antimicrobial and anti-biofilm formation activities of novel poly(vinyl alcohol) hydrogels reinforced with crosslinked chitosan and silver nano-particles. *Polymers* **2022**, *14*, 1619. [[CrossRef](#)] [[PubMed](#)]
26. Wang, J.L.; Xu, L.J. Advanced oxidation processes for wastewater treatment: Formation of hydroxyl radical and application. *Crit. Rev. Environ. Sci. Technol.* **2012**, *42*, 251–325. [[CrossRef](#)]

27. Crini, G.; Badot, P.M. Application of chitosan, a natural aminopolysaccharide, for dye removal from aqueous solutions by adsorption processes using batch studies: A review of recent literature. *Prog. Polym. Sci.* **2008**, *33*, 399–447. [[CrossRef](#)]
28. Wen, K.; Li, Y.; Zhang, S.; Zhang, X.; Han, R. Adsorption of congo red from solution by iron doped PVA-chitosan composite film. *Desalination Water Treat.* **2020**, *187*, 378–389. [[CrossRef](#)]
29. Kaur, R.; Goyal, D.; Agnihotri, S. Chitosan/PVA silver nanocomposite for butachlor removal: Fabrication, characterization, adsorption mechanism and isotherms. *Carbohydr. Polym.* **2021**, *262*, 117906. [[CrossRef](#)]
30. Elmehbad, N.Y.; Mohamed, N.A. Designing, preparation and evaluation of the antimicrobial activity of biomaterials based on chitosan modified with silver nanoparticles. *Int. J. Biol. Macromol.* **2020**, *151*, 92–103. [[CrossRef](#)]
31. Mohamed, N.A.; Al-harby, N.F.; Almarshed, M.S. Effective removal of Basic Red 12 dye by novel antimicrobial trimellitic anhydride isothiocyanate-cross-linked chitosan hydrogels. *Polym. Polym. Compos.* **2021**, *29*, S274–S287. [[CrossRef](#)]
32. Yagub, M.T.; Sen, T.K.; Afroze, S.; Ang, H.M. Dye and its removal from aqueous solution by adsorption: A review. *Adv. Colloid Interface Sci.* **2014**, *209*, 172–184. [[CrossRef](#)]
33. Wang, C.; Le, Y.; Cheng, B. Fabrication of porous ZrO<sub>2</sub> hollow sphere and its adsorption performance to Congo red in water. *Ceram. Int. Part B* **2014**, *40*, 10847–10856. [[CrossRef](#)]
34. Alharby, N.F.; Almutairi, R.S.; Mohamed, N.A. Adsorption behavior of methylene blue dye by novel crosslinked O-CM-Chitosan hydrogel in aqueous solution: Kinetics, isotherm and thermodynamics. *Polymers* **2021**, *13*, 3659. [[CrossRef](#)] [[PubMed](#)]
35. Al-Harby, N.F.; Almutairi, R.S.; Elmehbad, N.Y.; Mohamed, N.A. A novel O-carboxymethyl chitosan-based hydrogel of an outstanding adsorption performance for removal of cationic Basic Red 12 dye from its aqueous solution. *Polym. Eng. Sci.* **2023**, *63*, 2336–2353. [[CrossRef](#)]
36. Chang, M.Y.; Juang, R.S. Adsorption of tannic acid, humic acid, and dyes from water using the composite of chitosan and activated clay. *J. Colloid Interface Sci.* **2004**, *278*, 18–25. [[CrossRef](#)]
37. Baldez, E.E.; Robaina, N.F.; Cassella, R.J. Study of rhodamine b retention by polyurethane foam from aqueous medium in presence of sodium dodecylsulfate. *Sep. Sci. Technol.* **2009**, *44*, 3128–3149. [[CrossRef](#)]
38. Hu, H.; Liu, J.; Xu, Z.; Zhang, L.; Cheng, B.; Ho, W. Hierarchical porous Ni/Co-LDH hollow dodecahedron with excellent adsorption property for Congo red and Cr(VI) ions. *Appl. Surf. Sci.* **2019**, *478*, 981–990. [[CrossRef](#)]
39. Zenasni, M.A.; Meroufel, B.; Merlin, A.; George, B. Adsorption of Congo Red from Aqueous Solution Using CTAB-Kaolin from Bechar Algeria. *J. Surf. Eng. Mater. Adv. Technol.* **2014**, *4*, 332–341. [[CrossRef](#)]
40. Vimonses, V.; Lei, S.; Jin, B.; Chow, C.W.K.; Saint, C. Adsorption of congo red by three Australian kaolins. *Appl. Clay Sci.* **2009**, *43*, 465–472. [[CrossRef](#)]
41. Falaki, F.; Fakhri, A. Adsorption properties of nickel oxide nanoparticles for removal of Congo Red from aqueous solution. *J. Phys. Theor. Chem. Islam. Azad Univ. Iran* **2014**, *10*, 255–262.
42. Wang, L.; Wang, A. Adsorption characteristics of Congo Red onto the chitosan/montmorillonite nanocomposite'. *J. Hazard. Mater.* **2007**, *147*, 979–985, 2007. [[CrossRef](#)] [[PubMed](#)]
43. Karthikaikumar, S.; Karthikeyan, M.; Kumar, K.K.S. Removal of Congo Red Dye from Aqueous Solution by Polyaniline-Montmorillonite Composite. *Chem. Sci. Rev. Lett.* **2014**, *2*, 606–614.
44. Liu, Y.; Wang, W.; Wang, A. Removal of congo red from aqueous solution by sorption on organified rectorite. *CLEAN–Soil Air Water* **2010**, *38*, 670–677. [[CrossRef](#)]
45. Mumin, M.A.; Khan, M.M.R.; Akhter, K.F.; Uddin, M.J. Potentiality of open burnt clay as an adsorbent for the removal of Congo red from aqueous solution. *Int. J. Environ. Sci. Technol.* **2007**, *4*, 525–532. [[CrossRef](#)]
46. Ghribi, A.; Bagane, M.; Chlendi, M. Sorptive removal of congo red from aqueous solutions using raw clay: Batch and dynamic studies. *Int. J. Innov. Environ. Stud. Res.* **2014**, *2*, 45–56.
47. Patil, S.R.; Sutar, S.S.; Jadhav, J.P. Sorption of crystal violet from aqueous solution using live roots of Eichhornia crassipes: Kinetic, isotherm, phyto and cyto-genotoxicity studies. *Environ. Technol. Innov.* **2020**, *18*, 100648. [[CrossRef](#)]
48. Saha, P.D.; Chakraborty, S.; Chowdhury, S. Batch and continuous (fixed-bed column) biosorption of crystal violet by Artocarpus heterophyllus (jackfruit) leaf powder. *Colloids Surf. B Biointerfaces* **2012**, *92*, 262–270. [[CrossRef](#)]
49. Chakraborty, S.; Chowdhury, S.; Saha, P.D. Adsorption of Crystal Violet from aqueous solution onto NaOH-modified rice husk. *Carbohydr. Polym.* **2011**, *86*, 1533–1541. [[CrossRef](#)]
50. Khanam, N.; Uddin, M.T.; Islam, M.A. Adsorptive removal of Crystal Violet by Banyan leaf powder: Batch and Column Study. In Proceedings of the International Conference on Engineering Research, Innovation and Education, Sylhet, Bangladesh, 13–15 January 2017.
51. Saeed, A.; Sharif, M.; Iqbal, M. Application potential of grapefruit peel as dye sorbent: Kinetics, equilibrium and mechanism of crystal violet adsorption. *J. Hazard. Mater.* **2010**, *179*, 564–572. [[CrossRef](#)]
52. Kumar, R.; Ahmad, R. Biosorption of hazardous crystal violet dye from aqueous solution onto treated ginger waste (TGW). *Desalination* **2011**, *265*, 112–118. [[CrossRef](#)]
53. AL-Shehri, H.S.; Almudaifer, E.; Alorabi, A.Q.; Alanazi, H.S.; Alkorbi, A.S.; Alharthi, F.A. Effective adsorption of crystal violet from aqueous solutions with effective adsorbent: Equilibrium, mechanism studies and modeling analysis. *Environ. Pollut. Bioavailab.* **2021**, *33*, 214–226. [[CrossRef](#)]
54. Dada, A.O. Langmuir, Freundlich, Temkin and Dubinin–Radushkevich Isotherms Studies of Equilibrium Sorption of Zn<sup>2+</sup> Unto Phosphoric Acid Modified Rice Husk. *IOSR J. Appl. Chem.* **2012**, *3*, 38–45. [[CrossRef](#)]

55. Desta, M.B. Batch Sorption Experiments: Langmuir and Freundlich Isotherm Studies for the Adsorption of Textile Metal Ions onto Teff Straw (*Eragrostis tef*) Agricultural Waste. *J. Thermodyn.* **2013**, *2013*, 375830. [[CrossRef](#)]
56. Foo, K.Y.; Hameed, B.H. Insights into the modeling of adsorption isotherm systems. *Chem. Eng. J.* **2010**, *156*, 2–10. [[CrossRef](#)]
57. Naim, M.M.; Al-Harby, N.F.; El Batouti, M.; Elewa, M.M. Macro-reticular ion exchange resins for recovery of direct dyes from spent dyeing and soaping liquors. *Molecules* **2022**, *27*, 1593. [[CrossRef](#)] [[PubMed](#)]
58. Nandiyanto, A.B.D.; Hofifah, S.N.; Inayah, H.T.; Putri, S.R.; Apriliani, S.S.; Anggraeni, S.; Usdiyana, D.; Rahmat, A. Adsorption isotherm of carbon microparticles prepared from pumpkin (*cucurbita maxima*) seeds for dye removal. *Iraqi J. Sci.* **2021**, *62*, 1404–1414. [[CrossRef](#)]

**Disclaimer/Publisher's Note:** The statements, opinions and data contained in all publications are solely those of the individual author(s) and contributor(s) and not of MDPI and/or the editor(s). MDPI and/or the editor(s) disclaim responsibility for any injury to people or property resulting from any ideas, methods, instructions or products referred to in the content.